PHYSICAL PROCESSES IN STARBURST AND ACTIVE GALAXIES

HAGAI NETZER
School of Physics and Astronomy, Tel Aviv University, Tel Aviv 69978, Israel
E-mail: netzer@wise.tau.ac.il

The physics of the ionized gas in active galactic nuclei (AGN) is governed by the source luminosity, the spectral energy distribution (SED) and the gas density and distribution. Photoionization is the dominant heating and excitation mechanism throughout the central $\sim$ 1 kpc except for nuclear star-forming regions that are dominated by local heating processes. The physics of "pure" star-forming regions is very different. The energy input is mostly mechanical and the micro-physics of the ionized gas is governed by collisional processes. This review gives a short account of the steps required to construct photoionization and collisional models and apply them to three observed "regions" in AGN: the broad line region (BLR), the narrow line region (NLR) and the highly ionized gas (HIG). It also discusses the physical conditions in a typical starburst region. Specifying the gas distribution and properties in AGN reproduces the observed properties of all three regions, although extra ingredients, such as dust, are sometimes required. The emergent model is that of a "messy" AGN, with gas of different properties at almost all regions. The last part of this review deals with the AGN-starburst connection. It shows that both are intimately related in luminous AGN as well as in several ultra luminous IR galaxies (ULIRGs). New spectral tools are required to understand the physics of such objects. The most useful diagnostics for distinguishing accretion dominated from starburst dominated sources are likely to be found in the X-ray part of the spectrum.

1 The AGN Principle

Active galactic nuclei (AGN) are thought to be powered by accretion onto a massive black hole. The exact fraction of AGN among galaxies is not accurately known but recent studies suggest that it must be very large, especially if low luminosity AGN, such as LINERs, are taken into account. It is therefore tempting to present the *AGN Principle* (or, perhaps, the weak AGN principle) which states that *all galaxies contain active or dormant massive black holes.* Such a strong statement requires a proof. The present review is an attempt to look for part of this proof by studying the AGN-starburst connection.

The black hole mass is only one of the fundamental parameters determining the AGN properties. Mass accretion rate is a second important parameter. It is probably the main reason for the different appearance of LINERs, narrow line Seyfert galaxies and luminous quasars. Besides these two, there are various others that determine the observed AGN properties: the amount and

geometry of obscuring gas, the dust content and the size of the various emission regions are probably the most important of those. Any complete analysis must take all those into account. This review gives only a few of the more important manifestations.

No AGN review is complete without some terminology. I will only use the most common abbreviations such as the narrow line region (NLR), the broad line region (BLR), and the highly ionized gas (HIG). Only the simplest classification will be used throughout the chapters, avoiding, as much as possible, names such as Seyfert 1s, Seyfert 2s, LINERs and NLRGs. Instead I shall refer to type-I AGN (those objects showing broad, strong optical-UV emission lines in their spectrum), and type-II AGN (those showing prominent narrow emission lines and very faint, if any, broad lines).

The spectral energy distribution (SED) of AGN is complex, with significant differences between objects. Much of the complication can be avoided by describing it, over a restricted energy band, as a power-law in energy,

$$L_\nu = a\nu^{-\gamma} \ , \tag{1}$$

where a is a constant. This approximation is used for various energy bands by adding the relevant subscript to the power-law index γ, e.g. $\gamma_{\rm X}$.

2 The Physics of Ionized Gas

The physical properties of gas exposed to a strong radiation field are well described by photoionization theory. The time-dependent level of ionization, the time-dependent thermal structure, and the spectrum of the gas, are all well understood if the density is lower than about 10^{11} cm^{-3} and the emission lines are optically thin. Radiative transfer and high density processes are more difficult to treat and present-day calculations fall short of including all those in realistic AGN models. There are several books and comprehensive reviews that describe these processes, in particular Mihalas[?] , Osterbrock[?], Netzer[?] and Emerson[?]. Star-forming regions are thought to be powered by fast stellar winds and supernovae expanding shells. The spectrum is dominated by collisional processes and the time-independent equations, in the low density low optical depth limits, are easy to solve. Optically thick, high density collisional plasma is more difficult to treat and the time-dependent spectrum is still not well understood.

The following is a brief account of some of the principles, and the more important details necessary to analyze and compute the spectrum of starburst and active galaxies. The starburst part is less complete because it is covered

in other chapters. The reader is referred to the above mentioned references, and other reviews, for a more comprehensive discussion and additional details.

2.1 Photoionization

The fundamental time-dependent equation that describes the conditions in a gas situated at a distance r from a strong radiation source of monochromatic luminosity L_ν, is

$$\frac{dN_X}{dt} = -N_X[I_X + R_{X-1}] + N_{X-1}I_{X-1} + N_{X+1}R_X \ , \tag{2}$$

where N_X is the number density of ion X,

$$I_X = \int_{\nu_X}^{\infty} \frac{(L_\nu/h\nu)\sigma_\nu e^{-\tau_\nu}}{4\pi r^2} d\nu \tag{3}$$

is the ionization rate per particle, ν_X is the threshold ionization frequency of ion X, and

$$R_X = \alpha_X(T)N_e \tag{4}$$

is the recombination rate per particle. Auger ionization, collisional ionization, three-body recombination, and charge exchange reactions, were neglected for the time being. The additional requirement is

$$\Sigma N_X = N_{\rm element} \ , \tag{5}$$

where $N_{\rm element}$ is the total abundance.

The steady state solution is

$$\frac{N_{X+1}}{N_X} = \frac{I_X}{R_X} \ . \tag{6}$$

This leads to the definition of two important location dependent time scales: the recombination time, $1/R_X$, and the ionization time, $1/I_X$. The first gives the typical time required for ion $X+1$ to recombine to ion X, when the radiation source is suddenly turned off. The second is the time required for ion X to get ionized to ion $X+1$ after a large increase in the ionizing flux. The two can be quite different, depending on the radiation field and the gas density. Moreover, the coupling between the various stages of ionization suggests that, under various conditions, the fractional abundance of ion X may change very slightly, or remains almost constant, despite large changes in the radiation field (for more on these issues see Krolik & Kriss[?]). More interesting, perhaps, are the global recombination and ionization time scales, i.e. the time it takes for the entire atmosphere to get completely neutral or

Table 1. Various ionization parameters

Ionization parameter	E_1	E_2
U(hydrogen)	13.6 eV	∞
U(helium)	54.4 eV	∞
$U(\mathrm{X-ray})$	0.1 keV	10 keV
U(oxygen)	0.54 keV	10 keV

the time it takes for the ionization front to reach its equilibrium location. Both are close to $1/R_X$ where X is the most abundant ion of the element in question.

The level of ionization of photoionized gas can be described by the location-dependent value of the ionization parameter

$$U = \int_{E_1}^{E_2} \frac{(L_E/E)dE}{4\pi r^2 c N_{\mathrm{H}}} \ , \tag{7}$$

where c is the speed of light introduced to make U dimensionless. U is relevant only if E_1 is close to the minimum energy of photons that can significantly affect the level of ionization. Thus, for gas that is ionized by a soft-UV radiation, E_1 must be related to the UV ionizing field. This is normally taken at the Lyman limit and the appropriate name is U(hydrogen). On the other hand, the most suitable choice for gas whose level of ionization is dominated by a strong soft X-ray source is $E_1 \sim 1$ keV. The UV radiation of such a source may be very intense but the gas is transparent to such photons and U(hydrogen) has no real influence on the gas level of ionization. A good choice in this case is $E_1 = 0.54$ keV, corresponding to the K-shell threshold ionization of oxygen, the most abundant element controlling the conditions in highly ionized solar-metallicity gas. A suitable name is U(oxygen). Table 1 gives a list of four ionization parameters that are useful in various situations and Fig. **??** shows a typical SED for AGN with the various energies (E_1) used to define these ionization parameters. As a rule, using the "right" ionization parameter, we normally find that $U \sim 0.1$ corresponds to gas that produces strong emission lines in the energy range under question. For example, U(oxygen) = 0.1 results in strong 0.5-3 keV emission lines. A much smaller U results in neutral gas and a much larger U in gas that is so highly ionized that line emission, over the relevant energy range, is not significant.

The thermal structure of the gas is governed by a similar set of equations that involves energy terms like $(E - E_{\mathrm{threshold}})$. These are not given here and can be found in the various references mentioned earlier. The ionization and

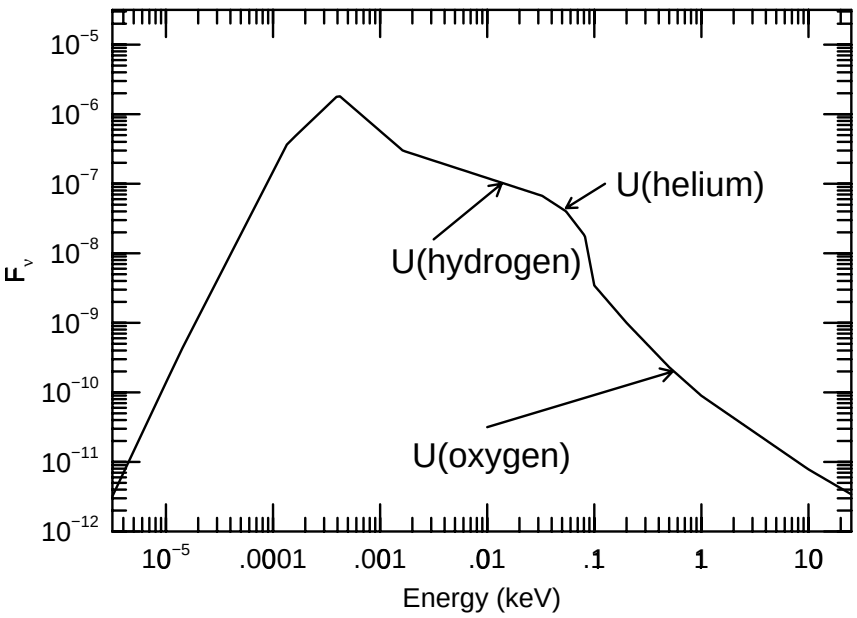

Figure 1. Theoretical spectral energy distribution (SED) for AGN and the various values of E_1 used to define the different ionization parameters.

thermal equations are, of course, coupled through the temperature dependence of the various atomic processes, such as the recombination and collisional ionization and excitation rates.

2.2 Collisional Processes and Shock-Wave Heating

In AGN, most of the emitting gas is photoionized by the central radiation field and collisions with fast particles do not play an important role in determining its level of ionization. This is very different from the conditions in X-ray bright starburst regions where the temperature can exceed several million degrees and most of the ionization is due to collisions with the fast electrons (see however comments in Sec. 6.4. regarding the photoionization of star-

forming regions in AGN). In this case, collisional ionization and radiative recombination are the dominant processes.

There are other situations where collisional processes play important roles in starburst and active galaxies. Small-scale jets in type-II AGN (e.g. the nuclear jet in NGC 1068) can transfer a large amount of mechanical energy into a very small region, producing strong shocks and bright emission from collisionally excited plasma[?]. Collisional ionization and three-body recombination, are affecting the level of ionization of the high density gas in the central accretion disk. Finally, the innermost part of the line emission region in AGN can attain such high densities that collisional ionization and three-body recombination cannot be neglected.

A comment about the general energetics of shock waves in AGN narrow line regions is in order. Fast moving shocks are capable of producing bright emission line condensation in the NLR[?]. Jets can be the most efficient in producing such shocks and, indeed, some models of the NLR[?] argue that the narrow line emission in Seyfert galaxies is powered entirely by radio-emitting jets. Such "photoionizing shocks" are powerful sources of ionizing radiation and the resulting spectrum is significantly different from the pure, single temperature collisional plasma spectrum.

As argued by Laor[?], the mechanical energy produced by the shock is roughly $(v^2/2c^2)m_{\rm shock}$ and the one produced by the black hole accretion is about $0.1m_{\rm accretion}c^2$. Observed NLR velocities are of the order of 500 km s^{-1} thus the ratio of the two is approximately $10^{-5}(m_{\rm accretion}/m_{\rm shock})$. For shock excitation to be energetically significant, the amount of shocked material must exceed, by many orders of magnitude, the amount of accreted material. However, much of the NLR gas seems to be gravitationally bound (see Sec. 4.3) and the loss of kinetic energy must also be associated with a loss of angular momentum. This must result in an inflow of the shocked gas into the center of the AGN and, eventually its accretion. This would lead to accretion luminosity which is orders of magnitude larger than the shock produced luminosity.

The argument can be applied, in a more quantitative way, to specific emission lines, e.g. the [O III] λ5007 line. A certain fraction of the shock energy is radiated as photons of this line and a certain fraction of the central source radiation is absorbed and re-radiated as 5007Å line photons. Comparing the two, leads to a similar conclusion: shock heating cannot contribute, significantly, to the emission lines in large accretion rate sources, unless most of the shocked gas is flowing out of the system. The accretion rate in faint AGN, in particular in LINERs, may be much smaller while the gas velocity is basically the same. Shock heating can play a more important role in such sources.

2.3 Additional Atomic Processes

The list of atomic processes mentioned so far is by no means complete. The following is a short reminder of other important processes.

Low temperature dielectronic recombination is important in gas whose level of ionization is determined by the UV radiation field. High temperature dielectronic recombination is important in collisional plasma. X-ray ionization from inner shells (Auger ionization) is important for ions with three or more electrons in strong X-ray radiation fields. The process couples non-adjacent stages of ionization and results in X-ray fluorescence lines that are commonly observed in the spectrum of AGN. Heating and ionization by secondary electrons must be considered when the gas is almost completely neutral and the radiation field contains hard photons. It increases the level of ionization (and the intensity of some lines, like Lyα) and reduces the cooling of the gas. Finally, charge exchange reactions, mostly with neutral hydrogen, are important in low ionization gas.

2.4 The Spectrum of Ionized Gas

The main "product" of photoionization and collisional plasma calculations is the predicted spectrum. This requires the solution of the time-dependent level population equations at every point in the cloud. For a two-level atom whose level-2 population is determined by recombination with rate $\alpha_{\rm eff}$, collisional excitation and de-excitation with rates q_{12} and q_{21}, and line (but no continuum) photon emission and absorption, the equations to solve are

$$\frac{dn_2}{dt} = n_1 q_{12} - n_2(A_{21}\beta_{21} + q_{21}) + N_{X+1} N_e \alpha_{\rm eff} \tag{8}$$

and

$$n_1 + n_2 = N_X \ , \tag{9}$$

where N_X itself is time-dependent (Eq. **??**).

In Eq. **??**, β_{21} is the "local escape probability", i.e. the probability of line photons to leave that location without being absorbed by level 1. This escape probability treatment replaces the more rigorous, full radiative transfer solution. It is introduced to enable a full local solution while general radiative transfer couples different locations and is, therefore, more complicated. A reasonable approximation is $\beta = 1/(1 + b\tau_{12})$ where b is a constant of order unity.

Having solved for n_1 and n_2, we can now express the line emissivity as

$$\epsilon_{21} = n_2 \beta_{21} A_{21} h\nu_{21} \ , \tag{10}$$

where, in general, ϵ_{21} is time dependent.

In AGN and starburst galaxies, emission lines are normally classified as either *recombination lines* or *collisionally excited lines*. Most of the observed hydrogen and helium lines belong to the first category, although collisional contributions to the Lyman and Balmer hydrogen lines, in high density AGN clouds, are known to be important. Most metal lines are collisionally dominated in photoionized and collisional plasmas. The exception is the soft X-ray (0.5–3 keV) lines in AGN that originate in photoionized gas (see below). The temperature in such a gas is far below the plasma equilibrium temperature and strong metal lines, like O VIII 653 eV, are mostly due to recombination (see however Nicastro et al.[?], regarding time dependent collisional processes in such a gas).

The equivalent width (EW) of recombination lines is used to deduce the *covering fraction*, C_f, measured in units of $\Omega/4\pi$, i.e. the part of the source covered by optically thick gas. This is easy to demonstrate by considering Lyα, one of the strongest emission lines in the spectrum. Under most circumstances, the number of Lyα photon is comparable (and in the simplest, recombination Case B conditions, identical) to the number of hydrogen ionizing photons. For a power-law continuum (Eq. **??**) extending from the Lyman limit to some high cut-off frequency $\nu_{\rm cut-off}$, this results in

$$\mathrm{EW}(L_\alpha) = \frac{1215}{\gamma}(\frac{3}{4})^\gamma[1-\nu_{\rm cut-off}^{-\gamma}]C_f \ \ \text{Å} \ . \tag{11}$$

A comparison with the observed equivalent widths of broad and narrow recombination lines suggests that, for the low temperature AGN gas, $C_f \sim 0.1$. For the HIG, the number is much larger and C_f is closer to unity.

Two additional processes leading to line emission need to be considered. The first is *continuum fluorescence*, sometimes referred to as photo-excitation or line scattering. This process is the result of populating level n_2 by absorbing the incident continuum. The process, that is not included in the simple two-level scheme of Eq. **??** (see Netzer[?] for the required modification) results in line emission whose intensity depends on the overall geometry. For example, in a static spherical configuration, or in a static spherical shell, where the continuum source is in the center, the emission due to this process is completely balanced by line of sight absorption, provided there is no additional opacity sources (e.g. a large disk or a large gas cloud around the center). The net emission in this case is zero. In a moving atmosphere, the emitted photons are Doppler shifted relative to the gas rest frame, and absorption and emission appear at different energies. This results in both emission and absorption whose equivalent widths are the same. Well known examples are

P-Cygni profiles in expanding stellar atmosphere and the X-ray spectrum of several type-I AGN.

Simple arguments can be used to estimate the relative intensity of continuum fluorescence lines and line emission due to radiative recombination. Both are related because, for a given ion and a strong resonance line, the bound-bound absorption cross section integrated over the line profile, and the bound-free absorption cross section integrated over the ground level continuum, are comparable. Since most recombinations lead to line emission, we find that for optically thin lines and continuum (this is the situation where continuum fluorescence is the most efficient), the relative number of line photons produced by the two processes is

$$\frac{\mathrm{N(continuum\ fluorescence)}}{\mathrm{N(recombination)}} = \frac{(\nu_l/\nu_o)^{-(\gamma+1)}(\pi e^2/mc)f_{12}}{\int_{\nu_0}^{\infty}(\nu/\nu_0)^{-(\gamma+1)}\sigma_\nu d\nu} \simeq$$
$$\simeq \frac{3+\gamma}{2}[\nu_{12}/\nu_0]^{-(\gamma+1)} \qquad (12)$$

For H-like and He-like ions, and a typical $\gamma \simeq 1$ continuum, the ratio is about 3. An important deviation is a situation where the line in question becomes optically thick and continuum fluorescence drops exponentially. Continuum fluorescence excitation of emission lines is thus strongly column-density and line-width dependent.

The second process is line fluorescence, i.e. line emission following the ejection of an Auger electron. The fluorescence efficiency depends on Z^3 thus the most abundant elements, like oxygen, do not produce strong fluorescence lines, compared with iron, despite the order of magnitude difference in abundance. This difference can partly be compensated by the larger incident flux around 0.54 keV (the K-shell threshold for neutral oxygen), compared with the flux near 7.1 keV (the K-shell threshold of neutral iron) in typical AGN.

Simple photon counting arguments, like those introduced for calculating the covering fraction and EW(Lyα) (Eq. **??**), can be used to estimate the EW of fluorescence lines relative to the incident continuum. Thus, the equivalent width of the 6.4 keV Kα line of iron can be calculated for a given SED and iron abundance. There are two practical differences. First, the column density required for complete absorption of the incident radiation is very large and, in some cases, a considerable part of the radiation is not absorbed by the gas. Second, the absorption at the relevant energy band (e.g. beyond the 7.1 keV threshold of neutral iron) is never due to only one element and Compton scattering is non-negligible too. Thus, not all of the absorbed photons, beyond a certain threshold, result in the emission of the fluorescence line in question.

The situation is much simpler when estimating the EW relative to the

scattered continuum. The reason is that, both the number of line photons, as well as the number of scattered continuum photons (against which the lines are measured) depends on the column density of the gas, provided it is Compton thin. For example, the EW of the strong 6.4 keV Kα line observed in AGN, assuming a power-law continuum with energy slope $\gamma_{\rm X}$, is

$$\mathrm{EW}(6.4\ \mathrm{keV}) \simeq 3.2[\frac{1.11^{-\gamma_{\rm X}}}{3+\gamma_{\rm X}}][\frac{\mathrm{F_Y}}{0.3}][\frac{n_{\rm Fe}/n_{\rm H}}{4\times10^{-5}}]\ \mathrm{keV}\ , \qquad (13)$$

where $\mathrm{F_Y}$ is the fluorescence yield (of the order of 0.3 for low ionization iron). There are small uncertainties on this estimate, to do with the metal abundances. There is also a viewing angle dependence[?] of EW(6.4 keV) that must be taken into account. However, the approximation is good enough to deduce the iron abundance ($n_{\rm Fe}$ in the above expression) in type-II AGN whose 6–7 keV continuum is thought to be dominated by reflection. The expression fails in situations where the Compton depth is large, and angle-dependent multiple scattering of the continuum photons must be taken into account[?,?] (Eq. 2).

2.5 A Cloud or not a Cloud?

Real computations require the definition of the basic line emitting entity which is normally referred to as a *cloud*. The assumption of clouds, or more generally condensations, is reasonable in view of spatially resolved observations of galactic HII regions. It is also required by line intensity considerations, mainly the observation that the typical line widths, in the BLR, are similar for low and high ionization lines. This is however problematic since such entities are either gravitationally bound or must be confined by external pressure. Self gravitating clouds must contain large amounts of gas. Most likely candidates are stars in the central cluster. These will be dealt with later under the name *bloated stars* (BS). Much lower mass clouds are normally assumed in the BLR. They can be as small as 10^{12} cm in diameter and contain as little as 10^{25} grams.

Confined clouds have been addressed in many papers but there is no real understanding of the confining medium or agent. The most likely possibilities are either thermal confinement, by a low density hot inter-cloud medium (HIM), or confinement by magnetic fields. The first has been discussed in numerous publications[?]. The idea is of a two-phase medium, where the hot and cold components are in pressure equilibrium. The HIM temperature is determined by Compton heating and cooling by the central radiation source. As pointed out by Mathews & Ferland[?] and many papers since, this results in a low temperature ($T \sim 10^7$ K) HIM with a large Compton depth, especially in high luminosity AGN. The resulting optical depth is too large to be

compatible with the observed variability of such sources. Relativistic HIM has also been suggested. In this case, the confining gas is of much higher temperature and the Compton optical depth significantly smaller.

An alternative and likely solution is magnetic pressure confinement[?]. In this case, $B^2/8\pi \geq NkT$ and the required magnetic field is of the order of one gauss for the BLR and much smaller for the NLR. Such magnetic fields are likely to occur near the central accretion disk and, perhaps, throughout the emission line region.

2.6 A System of Clouds

Adopted the cloud concept, we proceed in two stages. First to calculate the ionization and thermal structure for individual clouds. This results in the location-dependent cloud emission in the various emission lines, $j_{\rm line}(r)$ (erg $\rm s^{-1}$). We then integrate $j_{\rm line}(r)$ over volume taking into account the spatial distribution in properties (e.g. cloud size and shape) as well as absorption and obscuration by other clouds and by inter-cloud dust. In a spherical system, extending from $r_{\rm in}$ to $r_{\rm out}$, the total line emission is

$$E_{\rm line} = 4\pi \int_{r_{\rm in}}^{r_{\rm out}} n_{\rm c}(r) j_{\rm line}(r) \exp[-\tau({\rm line}, r)] r^2 dr \ , \qquad (14)$$

where $n_{\rm c}(r)$ is the radial dependent cloud number density and $\exp(-\tau({\rm line}, r))$ the absorption and extinction continuum optical depth, at the line energy, between location r and the observer. The computed $E_{\rm line}$ can be directly compared with the observations.

The above process must also include the computation of the bound-free and free-free emissions . In some situations (e.g. the Balmer continuum of the BLR clouds and the O VII and O VIII bound-free X-ray continua in the HIG) these provide additional diagnostics.

2.7 Diagnostic Diagrams

The observed line intensities can be used, in combination with the results of the calculations, to deduce the important physical parameters such as the ionization parameter, the gas temperature (in a collisional plasma) and composition. This is done by constructing line ratio or line diagnostic diagrams. The first give the line intensity as a function of ionization parameter (in photoionized gas) or temperature (in collisional plasma). The second convey the same information by plotting one line ratio against another. Fig. **??** shows an example that can be applied to X-ray lines in photoionized AGN gas.

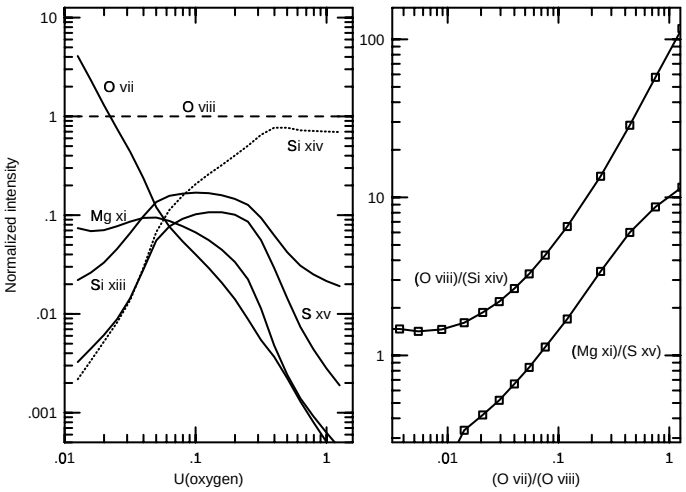

Figure 2. Left: An X-ray line ratio diagram, as a function of U(oxygen), for a low density ($N_{\rm H} = 10^5$ cm^{-3}) solar metallicity, low opacity photoionized gas. Right: Two diagnostic (line ratio) curves for the same gas. The combination of several such diagrams can be used to solve for both the ionization parameter and the gas composition.

2.8 Limitations and Uncertainties

While present photoionization computations are very advanced, there are several known limitations:

Reliable and unreliable line calculations: Most strong broad AGN lines are very optically thick. Such lines are normally treated with the escape probability formalism even in the most advanced photoionization codes. As explained, this treatment is local in nature and line transfer is not treated in detail. The local escape probability method is probably adequate for treating the high ionization lines like C IVλ1549 and N Vλ1240, the recombination lines like He IIλ1640, intercombination lines like C III]λ1909, and perhaps also for Lyα. It is definitely inadequate for the hydrogen Balmer lines and, perhaps, also for calculating the intensity of lines of low ionization ions like Fe^+ and Mg^+. It is also limited in its

treatment of the angular emission pattern of large optical-depth lines. Full radiative transfer methods, combined with detailed ionization and thermal treatment, must be used to verify the accuracy of the present calculations. Such codes are not yet available.

Time-dependent spectra: While time dependent line emission in AGN must be important, because of the large continuum variations, a full time-dependent treatment of the spectrum is still lacking (see however a time-dependent treatment of the NLR gas[?,?]).

Cloud distribution: Cloud confinement is still a major problem and the cloud distribution is still unknown. Regarding the latter, two different possibilities have been considered. The first[?] is a simple spherical cloud system, where there is one type of cloud at every distance. An example is given in the following section. The second is the locally optimally emitting clouds (LOC) model[?,?], that assumes numerous clouds, with a range of density, column density and covering fraction, at any given location. The main idea of the model is that the local ionizing flux, and the gas density, produce a large range of ionization parameter at any given location. Lines from high and low ionization species are produced, with different efficiencies, at all radii, and the local spectrum reflects the range of physical properties. The $1/r^2$ central-source flux variation is the main reason for the different contributions to the various emission lines at different locations. In the LOC model, the general tendency is for lines of higher ionization and higher critical density to be emitted closer to the center.

2.9 The Motion of Ionized Gas

The equation of motion for ionized gas includes three major terms, gravity, $g(r)$, radiation pressure acceleration, $a_{\rm rad}(r)$, and drag-force. Gravity dominates in almost all cases of low ionization, large column density gas. However, for highly ionized gas in strong radiation fields, acceleration by radiation pressure force can be very efficient and dominates over gravity and drag forces.

The radiation pressure force is obtained by summing over the contributions from various ions. The contribution due to ion X is

$$a_{\rm rad}(r,X) = \frac{N_X}{\rho(r)c}\int_{\nu_X}^{\infty}\frac{L_\nu\chi_\nu e^{-\tau_\nu}}{4\pi r^2}\,, \qquad (15)$$

where χ_ν is the total absorption cross section. Assuming an average ionizing energy $\overline{h\nu}$, an absorption cross section which is dominated by bound-free

processes, and using the definition of I_X from Eq. **??**, we find $a_{\rm rad}(X) \propto \overline{h\nu} N_X I_X / N_e$. For a steady state gas, photoionization is exactly balanced by radiative recombination and $N_X I_X = R_X N_{X+1}$. Thus $a_{\rm rad}$ is proportional to N_{X+1} and for the specific case of hydrogen, $a_{\rm rad}({\rm total}) \propto N_e$.

It is customary to introduce the "force multiplier", $M(r)$, which is the ratio of the total radiation pressure to the Compton radiation pressure

$$M(r) = \frac{a_{\rm rad}({\rm total}, r)}{a_{\rm rad}({\rm Compton}, r)} \ , \tag{16}$$

where

$$a_{\rm rad}({\rm Compton}, r) = \frac{N_e(r)\sigma_{\rm T} L_{\rm total}}{4\pi r^2 \rho(r) c} \ , \tag{17}$$

and $\sigma_{\rm T}$ is the Thomson cross section. Obviously, $M(r) \geq 1$ by definition.

The main contributions to $M(r)$ are from bound-bound and bound-free transitions. The former dominates in all cases where the line optical depths are small. In such cases it contributes between 50 and 90% of the total radiation pressure. In other situations, some or all of the resonance lines are optically thick and the bound-bound contribution is reduced with the increased line opacity. Fig. **??** shows an example of the various contributions to the force multiplier in a highly ionized AGN gas[?].

3 The Broad Line Region

Having established the general principle, we can now examine different "regions", i.e. various combinations of cloud location, gas density and column density. A complete description of the specified region includes also its boundaries, the gas dynamics and additional components (e.g. dust) that can be found within these boundaries. Such regions may or may not exist in real AGN and observations must provide the ultimate test.

3.1 The BLR Spectrum

First we consider a situation where the gas density is of order 10^{10} cm^{-3}, the column density is 10^{22-23} cm^{-2}, and the location a few light-days from the center. For a low luminosity AGN, this would imply U(hydrogen) $\sim 10^{-2} - 10^{-1}$ which means that the dominant carbon ion is C IV, the dominant oxygen ions are O VI, O V and O VI, etc. Such clouds must emit strong optical and UV lines of moderately ionized carbon, nitrogen and oxygen, as well as strong Lyman and Balmer hydrogen lines. The large column density also suggests that, if the internal gas motion is mostly thermal, all metal lines, as

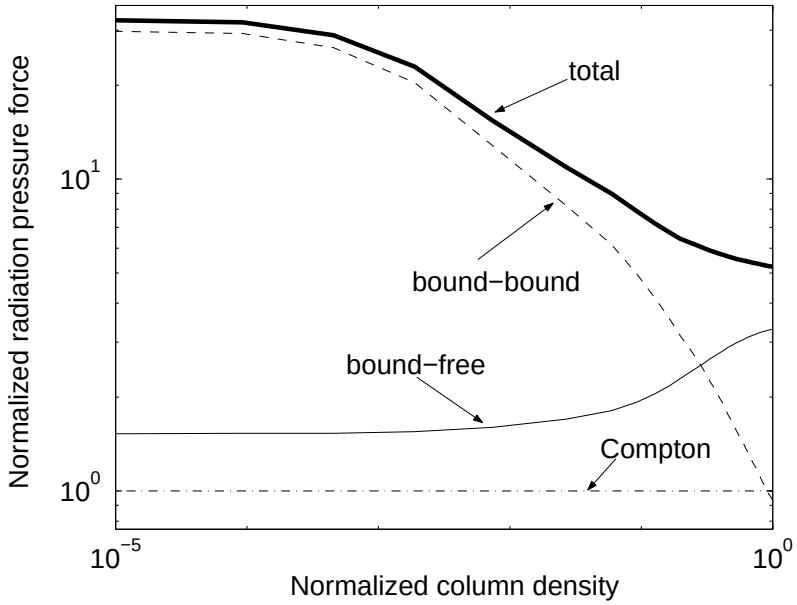

Figure 3. Contributions to the radiation pressure force at various depths inside a highly ionized AGN cloud of column density 10^{22} cm^{-2} and U(oxygen) = 0.01 at the illuminated face. From Chelouche & Netzer[?] ©2001 Blackwell Sci.

well as the Lyman and Balmer lines, have large optical depths. Combined with the large Keplerian velocities corresponding to this location, the predicted spectrum is of broad strong emission lines. This is, indeed, observed in AGN and is known as the BLR. Fig. **??** shows a composite BLR spectrum.

The general BLR properties have been reviewed, in great details, in several books and articles[?,?,?,?,?] and the following is only a short account of some of the most important issues.

3.2 Line Intensity and Line Profiles

Present day photoionization models are quite successful in explaining many of the observed properties of the BLR gas. In particular, there is a good agreement between the mean value of U(hydrogen) required to explain the observed line intensities and the emissivity-weighted-radius of the BLR which,

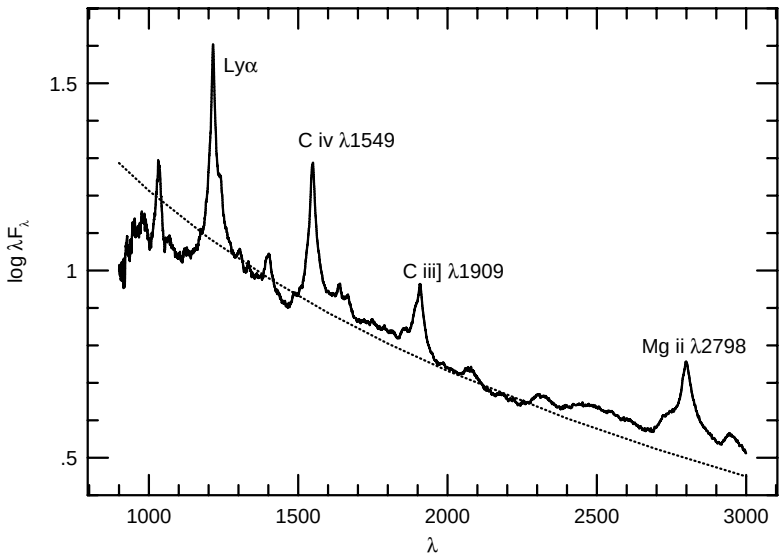

Figure 4. A composite AGN spectrum obtained by adding spectra of several quasars. The dotted line is a power-law continuum with $\gamma_{\rm UV} = 0.6$. Note the turnover of the continuum, at short wavelengths, relative to the power-law. Courtesy of A. Laor.

for the Balmer lines is given by

$$R_{\rm BLR}({\rm Balmer}) \simeq 0.15 L_{46}^{0.7} \ {\rm pc}, \tag{18}$$

where $L_{46} = L_{\rm ionization}/10^{46}$ erg s^{-1}. This expression, which is obtained from the reverberation mapping of 34 AGN[7] with the additional assumption that $L_{\rm Bolometric} = 9\lambda L_\lambda(5100\text{Å})$, suggests that the physical conditions in BLR clouds do not scale linearly with $L^{1/2}$. In particular, it suggests that, in the BLR,

$$U({\rm hydrogen}) \propto L_{\rm ionization}^{-0.4} \ , \tag{19}$$

which means that, on the average, the BLR gas in low luminosity AGN is more ionized compared with the gas in higher luminosity sources. This interesting

conclusion must be tested for high ionization lines, like C IV λ1549, since the result only applies to the hydrogen Balmer lines[?] .

Another success of the models is the realization of a thick geometry, i.e. the understanding that $r_{\rm out} \gg r_{\rm in}$. A detailed mapping of the BLR requires specific assumptions about the gas distribution, as illustrated below. A notable exception is the relative intensity of the Balmer and Lyman hydrogen lines which cannot be explained by present day models. This problem, first raised by Baldwin[?] and discussed extensively in the literature, is related to the large observed intensity of the Balmer lines, far in excess of their predicted intensity.

3.3 Energy Budget and SED

Among the few open issues regarding the BLR spectrum are the *energy budget* and the SED problems. Both are related to the fundamental assumption that the observed Lyα flux represents, to a high degree of accuracy, the total number of ionizing photons (Eq. **??**). Similar arguments suggest that the observed flux of the HeII lines is a good measure of the $E > 4$ Rydberg continuum since most of the radiation at those energies is absorbed by He^+. Thus, several observed lines give indications for the number of unobserved Lyman continuum photons as well as on the shape of the unobserved UV continuum. Given this assumption, the covering factor can be deduced from the measured equivalent widths of the hydrogen and helium lines.

However, years of observations and great improvement in AGN modeling cannot reconcile the discrepancy between the observed SED and the equivalent widths of the recombination lines. The observed SED seems to be under luminous to explain the observed line intensities and too soft to explain the observed line ratios. It seems that, either the far UV continuum is very different from the one obtained from the extrapolation of the optical-UV continuum (which is a problematic assumption by itself since, in some high redshift sources, much of the Lyman continuum is directly observed) or there is a fundamental flaw in the models.[?,?,?].

3.4 Gas Composition

An interesting development of the last decade[?] is the realization that AGN metallicity, that was suspected to be high, as expected in galactic nuclei, is indeed unusual at least in high luminosity sources. The unusually high abundances are deduced from comparing strong UV lines, such as N V λ1240, with recombination lines such as He II λ1640. The enhancement is more noticeable for secondary elements like nitrogen. The recent study of lower luminosity

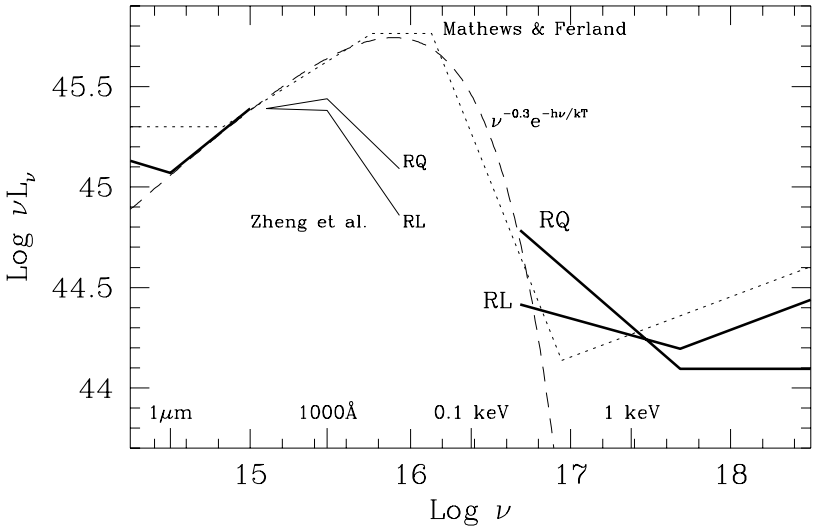

Figure 5. Several theoretical SEDs compared with real observations at optical-UV and X-ray energies. The extrapolated X-ray flux meets the observed UV continuum and does not require the "big blue bump" marked by the dashed lines. Courtesy of A. Laor.

PG quasars[?] suggests a similar behavior in those sources and, perhaps, a luminosity dependence of the composition of the line emitting material. All this hints to the suggestion that luminous AGN are related to intense star-forming activity. Obviously, there are interesting implications to galaxy and black hole evolution.

3.5 Mapping the BLR

The great advance in applying reverberation mapping to AGN observations (see Brad Peterson's review in this book), enables, for the very first time, a meaningful attempt to map the ionization and mass distribution in the BLR in several low luminosity AGN. The following is a brief account of the latest results based, primarily, on Kaspi & Netzer[?] and Korista & Goad[?].

A recent work by Kaspi & Netzer[?] presents an attempt to model, in detail, the time-dependent line and continuum variations across the BLR, in the well studied case of NGC 5548. The observations of this galaxy are par-

ticularly useful since they include well sampled light curves of the optical and UV continuum, as well as about eight isolated emission lines. This is essential for checking the consistency of the emission line models since various emission lines respond differently to the ionizing continuum variations. The model assumes a simple radial distribution of spherical, constant density clouds and requires seven parameters: the inner and outer radii, the radial particle-density parameter, s, defined by

$$N_{\rm H}(r) \propto r^{-s} \ , \tag{20}$$

the cloud number density parameter, p, defined by

$$n_{\rm c}(r) \propto r^{-p} \ , \tag{21}$$

the normalization of the density and column density at a given radius, and the global normalization of the covering factor (i.e. the total line emission). A modified version includes, also, a variable-shape SED which adds one or two more parameters. Since the clouds are assumed to be spherical, and the cloud mass is conserved, it is easy to obtain also the specific radial dependences of the column density, the cloud radius, the ionization parameter and the covering factor that are all related to s and p.

The calculations[?] do not attempt to fit the Balmer line light curves because of the uncertainty in calculating the transfer of these photons. Similarly, there is no attempt to calculate the FeII and MgII line intensities. There are four UV lines that are modeled (Lyα, He II λ1640, C III]λ1909 and C IVλ1549) and the results are in good agreement with the observations provided $1 \lesssim s \lesssim 1.5$ and $p \gtrsim 1.5$. Other important results include a lower limit on the column density of the BLR clouds, a well defined range of acceptable densities. The results of the fitting to the light-curves of the four emission lines are shown in Fig. **??**.

In a parallel effort, Korista & Goad[?] constructed a LOC model in attempt to fit the observed light curves of the very same source. As explained, the LOC model assumes a very different gas distribution with a large range of properties at any given location. The current version of the model requires eight parameters (some of which are fixed and others allowed to vary) that describe the density, column density and covering fraction at any chosen location. The model fits reasonably well the observed time-dependent fluxes of the four lines modelled by Kaspi & Netzer[?], and fails, like the other model, to explain the Mg IIλ2798 line intensity.

Given the above two attempts, and various other works underway to improve the models, and to fit the spectrum of other sources, we conclude

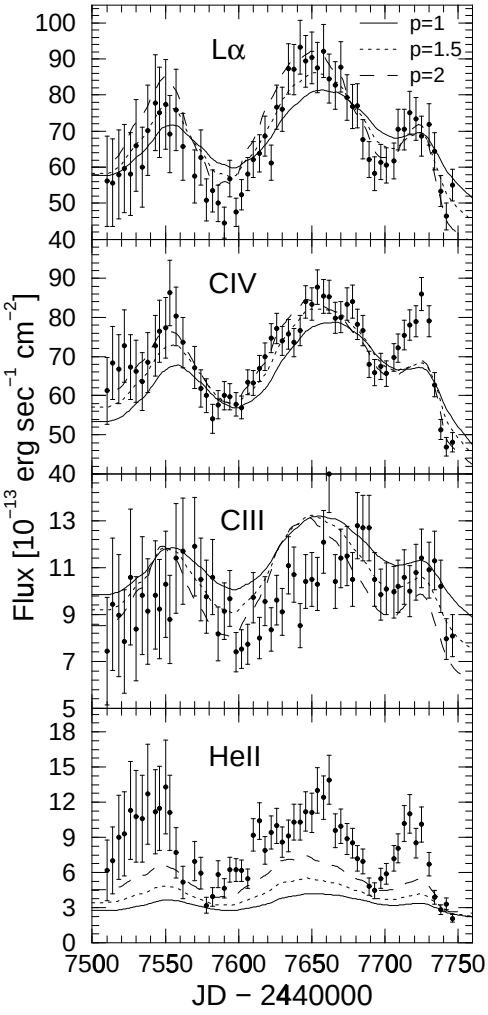

Figure 6. Observed (points with error bars) and calculated (smooth curves) light curves for NGC 5548, under various assumed conditions on the cloud number density parameter p. From Kaspi & Netzer[7] ©1999 AAS.

that AGN-BLRs are reasonably well understood although outstanding issues still remain.

3.6 Bloated Stars as BLR Clouds

The idea that stars in the (hypothetical) nuclear cluster can absorb and reprocess the AGN continuum radiation, is not new. It has been discussed in various papers[?,?,?,?] since the early 1980s and studied, in much greater details recently[?,?,?]. The most recent version of the model is based on the suggestion that the broad emission lines are emitted from the winds or the mass-loss envelopes of giant stars in the central cluster. These have been named *bloated stars* (BS) and while their origin and formation is not entirely understood, there are reasons to believe that they can evolve in the extreme environment near the central black holes. Models involving the emission of strong lines from the cometary tails of such stars, or their tidally disrupted atmospheres, have been discussed in various levels of detail.

The challenge of the BS model is to explain the various observed BLR properties. In particular, the observed broad line intensities, profiles and variability must be reconstructed by the model. Several papers[?,?,?] go a long way in this direction, although significant problems remain. A major advantage of the model is the removal of the confined cloud hypothesis. A major disadvantage is the predicted small number of BSs. The reason is that, such highly evolved stars cannot represent more than a tiny part of the nuclear stellar populations. Since the number of BSs can be estimated from the observed line intensity and covering fraction, there are strong limits on the total stellar population. Stellar collisions are expected too (this presents a problem for all cloud models) and there are other difficulties. A fundamental difference between the BS model and the cloud model is the total mass. A single BS can be more massive than 10^8 "standard" BLR clouds. The BS model requires, therefore, much more mass in the BLR.

3.7 The Number of BLR Clouds

High spectral resolution observations suggest that, in general, the observed emission line profiles are smooth over thousands of km s^{-1}. For example, the very detailed observations of low luminosity sources like NGC 4151, clearly demonstrate that, if the line profiles are produced by small individual clouds, the deviation from a smooth flow or motion is extremely small[?]. The observed deviations from a smooth profile, with assumptions on the velocity field, can be used to deduce the number of clouds. Arav and collaborators[?] have used such arguments to argue that, if individual clouds emit pure thermal line

profiles, the number of clouds is huge. For the specific case of NGC 4151, their Monte-Carlo simulations suggest at least 10^7 clouds.

While the smooth line profiles are problematic for all cloud models, this is specifically noticeable in the bloated star model where the expected number of stars is only about 10^{4-5}. There are several suggestions of how to reconcile the observed profiles with a much smaller number of clouds. One possibility is that internal motions (the so-called microturbulences) are super-sonic, reaching[?], perhaps, several hundred km s^{-1}. For BSs, the suggestion is that cometary tails, resulting from tidal forces in the vicinity of the central black hole, are associated with large internal differential velocities. This helps to reduce the number of clouds. It also introduces other difficulties, such as the dramatically reduced line optical depth in the presence of large turbulent motions.

4 The Narrow Line Region

Next we consider lower density gas, $N_{\rm H} \sim 10^{3-5}$ cm^{-3}, at larger distances, up to about 1 kpc, with typical dimensions of several hundred parsecs. This would give an ionization parameter which is similar, or perhaps slightly smaller, than the one deduced for the BLR. Scaling the Keplerian velocities with the increased distance, we anticipate narrower emission lines of FWHM= few$\times$100 km s^{-1}. The appropriate name would be the *narrow line region* (NLR).

4.1 The NLR Spectrum

The main expected spectral difference between the BLR and the NLR (except, of course, for the line width) is the presence, in the NLR, of strong forbidden lines, as a result of the lower density. The relative intensity of the NLR and BLR lines, assuming ionization bounded clouds in both regions, reflects the relative covering factor of the two regions. A rough estimate can be obtained by comparing the relative intensity of the broad and narrow Hβ line components. In many type-I AGN, the narrow component of the Hβ line is an order of magnitude weaker than the broad Hβ component. We expect this to be also the ratio of the covering factors in the two regions. As explained below, this is not necessarily the case if other ingredients, such as dust, are included.

The NLR is, perhaps, the best observed region in active galaxies. In nearby sources it is spatially resolved, thus a location-dependent velocity map can be obtained. The brightness of the NLR in nearby sources allows high quality optical, UV and IR observations and, starting from 1999, also real X-ray spectroscopy. Figs. **??**- **??** show the narrow line spectrum of various

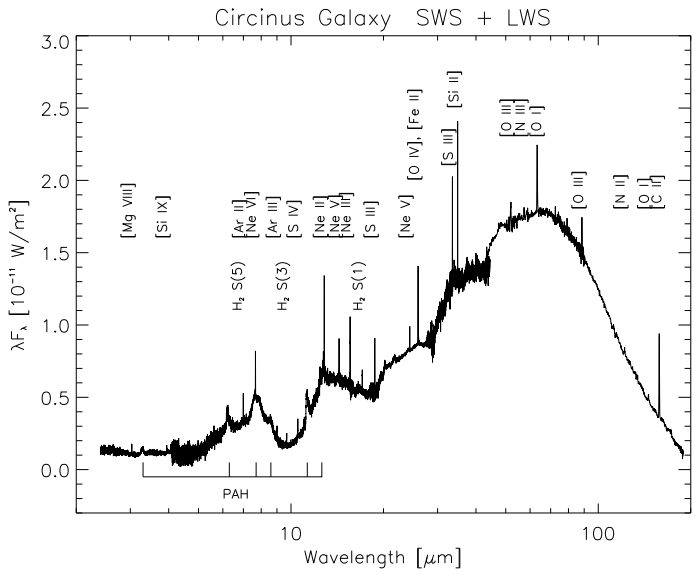

Figure 7. The ISO SWS+LWS spectrum of the Circinus galaxy. Courtesy of E. Strum.

AGN in various wavelength bands.

Some of the most important characteristics of the spectra are worth commenting on.

- Many of the observed optical, UV and IR lines seem to originate from the same NLR clouds. Given this, we can infer the physical conditions in the gas with great accuracy because (a) the lines are easy to interpret (low density, no complicated radiative transfer); (b) we can observed many lines and hence deduce the important parameters of density, temperature and abundance using standard line ratio techniques, and (c) the required reddening corrections can be obtained by comparing reddening sensitive line pairs such as the Balmer and Paschen hydrogen lines (see however a comment below about internal and external dust). The main problem is that the spatial resolution of present day mid-IR instruments (e.g. ISO) is

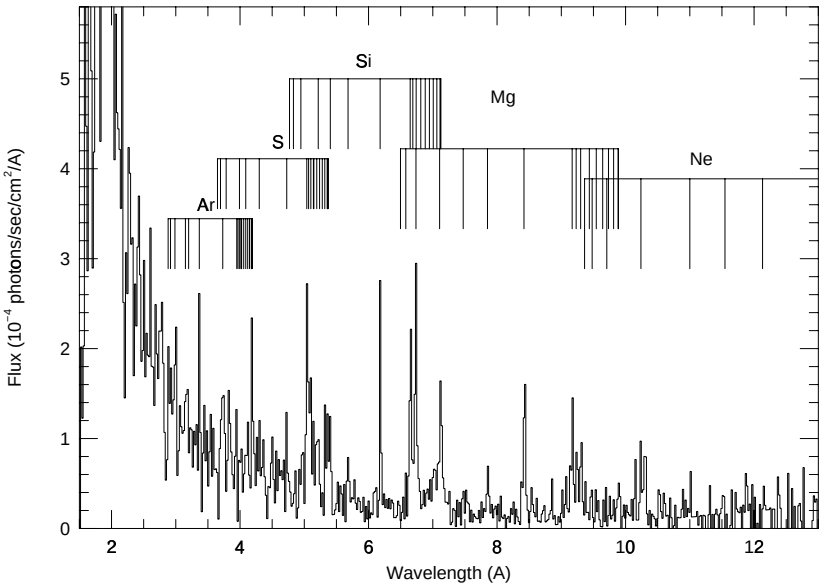

Figure 8. The *Chandra* X-ray spectrum of the Circinus galaxy. From Sambruna et al.[?] ©2001 AAS.

inferior to that of the large ground-based telescopes and the HST. Thus, only global reddening corrections can be obtained by using the mid-IR lines.

- Some mid-IR emission lines (e.g. [NeVI]7.66μm) as well as optical lines due to Fe X, Fe XI and Fe XIV, clearly originate in clouds of very high level of ionization. These *coronal lines* are probably ionized by the same central continuum, although there are alternative explanations involving collisional ionization in a much hotter environment[?]. In several well studied cases, there are clear signs of different dynamics of the coronal line region that suggest that this part of the NLR is closer to the central source and is characterized by higher than average density and velocity.

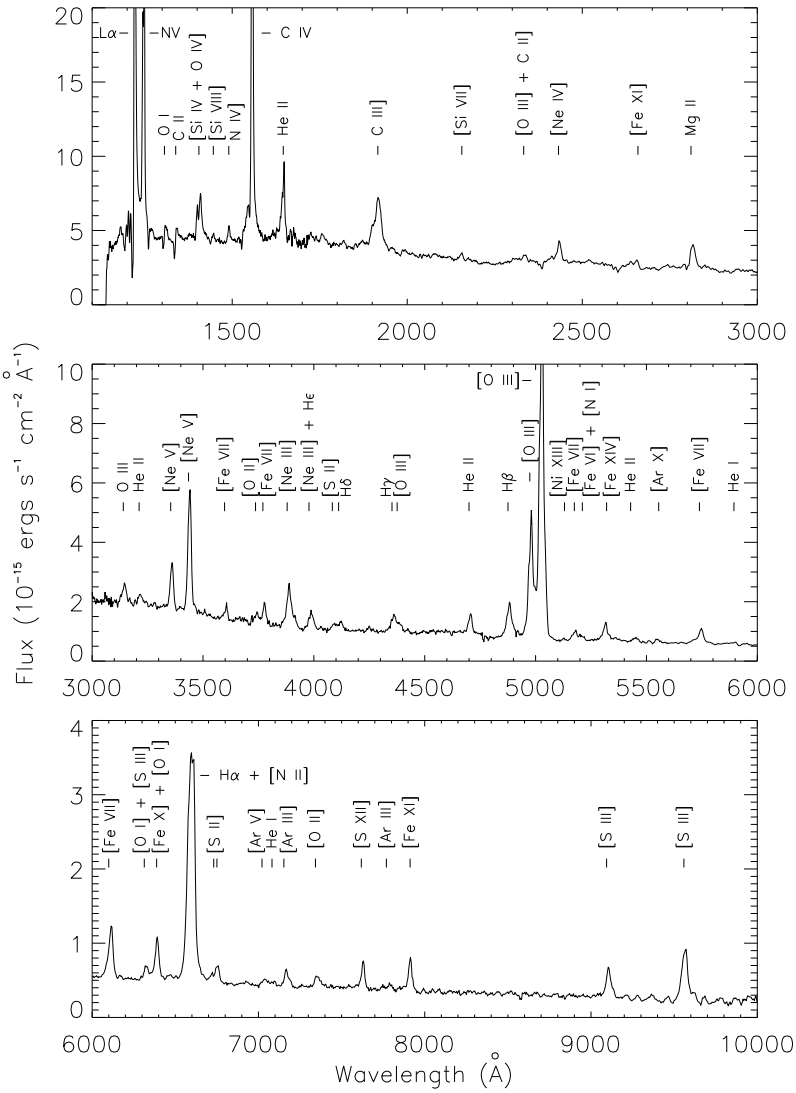

Figure 9. An HST spectrum of a hot-spot in NGC 1068. From Kraemer & Crenshaw[?] ©2000 AAS.

Thus, in at least several sources, the NLR is stratified with both density and ionization decreasing outwards. In the simple radial-dependent cloud model, this means $s < 2$ (Eq. **??** but note, again, the alternative LOC model[?]).

- The ISO observations of starburst and active galaxies[?,?] clearly show the presence of strong PAH (polycyclic aromatic hydrocarbon) features, mostly at around 7.7 and 8.6 μm. While the physics and chemistry of these small molecules is not very well understood, it is believed that they are sensitive to high energy (far UV and soft X-ray) radiation that can easily destroy them. The EW of the PAH features is argueably a good measure of the strength of the unobserved continuum radiation. Indeed EW(PAH) seems to be larger in starburst galaxies compared with AGN (see however an alternative[?] analysis). Such spectral features are useful in determining the ionizing flux in the NLR, even in highly obscured sources. Present observations are consistent with the idea that the line emitting part of the NLR is illuminated and excited by the central source in the direction where there is a clear view of the center. NLR-type clouds that are shielded from the central source (if such clouds exist) do not emit detectable narrow lines.

- The narrow X-ray lines in type-II AGN (only two published results, correct to October 2000) come from a region which seems to overlap with the NLR but with very different properties. Evidently, some of the nuclear gas is extremely highly ionized and while occupying the same volume, it is not necessarily of the same origin. This highly ionized gas (HIG) is further discussed in Sec. 5.

4.2 Dusty NLRs

Like all known HII regions, dust is likely to be present in AGN emission line regions. Such dust will scatter and absorbe some of the ionizing and non-ionizing radiation, and will affect the observed spectrum. There is clear evidence for dust in the NLR, obtained by comparing narrow emission lines of known relative intensity and very different wavelengths. However, there is no indication for dust mixed in with the BLR gas. It is likely that the harsh environment of the BLR, mainly the strong radiation field, is the reason for this deficiency. As explained below, this is also supported by other observations.

A comparison of the broad and narrow Balmer lines suggests, based on simple photon-counting arguments, that if the gas in both regions is optically thick in the Lyman continuum, the covering factor of the BLR is an order of

magnitude larger than the covering factor in the NLR. Moreover, counting the number of the narrow Hβ line photons, shows them to be very small considering the expectation, only about 1% of the expected number given the NLR geometry. This is entirely inconsistent with estimates of the (hypothetical) cone opening angle (see R. Goodrich contribution) and direct mapping of the NLR, by HST, in nearby sources. A possible explanation is that the NLR gas entirely fills the open cone but is mostly optically thin and does not absorbe a large fraction of the ionizing continuum. This is in conflict with several observed line ratios as well as the emission measured in some of the lines.

An alternative explanation for the "missing" NLR gas is the presence of dust in most of the volume outside the BLR[?]. If AGN dust is of similar composition as the interstellar dust in our own galaxy, we can calculate the dust sublimation radius, i.e. the minimum radius where dust of a certain composition can survive the central radiation field and does not evaporate. For graphite dust particles, this radius is given roughly by

$$R_{\rm sub} = 0.2 L_{46}^{1/2}\,{\rm pc}\,. \tag{22}$$

Evidently, $R_{\rm sub} \simeq R_{\rm BLR}$ which suggests that there is a natural boundary to the BLR. According to this explanation, the entire volume, from a small fraction of a parsec, very close to the central black hole, to hundreds of parsecs from the center, is filled with gas whose average density is a decreasing function of distance. The inner $R_{\rm sub}$ parsecs are void of dust since any dust particle that could have formed there, evaporates on a short time scale. In this region, almost all of the ionization radiation is absorbed by gas.

The presence of dust in the NLR, just outside $R_{\rm sub}$, can substantially change the level of ionization. Such dust, referred to as *internal dust*, competes, effectively, with the ionization of the gas since the dust particles have large absorption cross sections at all energies between about 0.02μm and 10μm. The fraction of Lyman continuum photons absorbed by the dust, relative to those absorbed by the gas, is proportional to U(hydrogen) since

$$\frac{N_{\rm dust}}{N_{\rm H^0}} \propto \frac{N_{\rm H^+} + N_{\rm H^0}}{N_{\rm H^0}} \propto U({\rm hydrogen})\,. \tag{23}$$

Therefore, dust is more efficient in attenuating the ionizing radiation in highly ionized gas, where it absorbs a larger fraction of the photons capable of ionizing the gas. The different ionization structures of dusty and dust-free environments are illustrated in Fig. **??** that shows the shrinking of the HII part of the dusty gas. This involves weaker emission lines.

For AGN, the suggestion is that the gas just outside the BLR is dusty and characterized by a large ionization parameter which results in inefficient

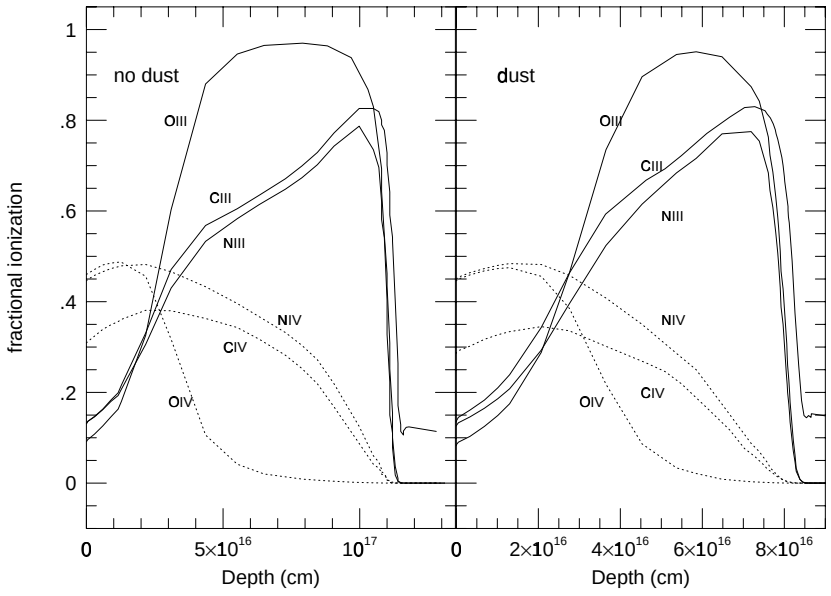

Figure 10. The effect of internal dust on the level of ionization, and the depth of the ionization front, inside a typical NLR cloud. In this case, U(hydrogen) = 0.01 and the gas-to-dust ratio is similar to the mean interstellar value. Note the shrinking of the HII region size by about 30% but the very similar ionization structure.

line emission. Moreover, such dust has great influence on the emissivity of Lyα and other resonance lines that suffer additional attenuation because the effective dust opacity in those wavelengths is greatly enhanced (by a factor of ~ 5) due to the large number of scattering of the line photons. The result is that highly ionized dusty regions emit weaker emission lines.

As stated earlier, this review is concerned with the consequence of having gas of certain properties at certain distances from a typical AGN continuum source. In Sec. 3 we found that such a combination produces the standard BLR and in this section we illustrated how a different combination produces the standard NLR. It is therefore interesting to note that NLR gas, mixed with

dust, can explain the *absence* of *intermediate line region* in AGN (a statement challenged by some AGN observers). The combination of gas density at the location where the gas velocity is intermediate between the BLR and the NLR velocities, does exist. However, if the above explanation is correct, the emission lines produced in this region are extremely weak because of the dust. This leads to the apparent absence of such regions in AGN.

4.3 The Motion of the NLR Gas

The dynamics of the NLR gas has been studied extensively, but the results are still inconclusive[?]. Optically thick NLR clouds are likely to be dominated by the gravitational field, because of the large amount of neutral gas. Indeed, typical observed widths of narrow emission lines are similar to what is expected given the bulge mass of the parent galaxy. Radiation pressure force must be important for the dynamics of those NLR clouds with little or no neutral gas. The velocity of such a gas is likely to be dominated by a large outward component. Unfortunately, it is not simple to tell them apart.

Observations of narrow emission lines clearly indicate that some narrow line profiles, especially in lines of highly ionized species, exhibit strong blue asymmetry. This is particularly noticeable in almost all coronal lines in many AGN. The asymmetry can be due to either an expanding atmosphere whose receeding part is partly obscured, or from infalling clouds that are very faint when observed from their neutral back side (far from the central source). The most likely opacity source in such clouds is internal dust. Recent ISO observations seem to give the first clue to the origin of the blue asymmetric narrow lines. The comparison of optical and IR lines of the same ion, enables to test the effect of dust since the IR lines are hardly affected by reddening[?]. Thus if dust is present, and causing the blue asymmetry in the optical line profiles, this will not be seen in the IR line profiles. The conclusion, after studying several IR-optical line pairs in two AGN, is that the same blue asymmetry is observed in the IR lines, suggesting that the blue asymmetry is not due to internal dust. It seems that the NLR gas, at least the highly ionized clouds in those sources, is flowing outward at high velocities. A plausible (but not the only) explanation for the blue asymmetry is central obscuration, perhaps by the central accretion disk.

4.4 Recovering the SED

The combination of a large number of UV, optical and IR narrow emission lines is also useful in recovering the unobserved (far UV) part of the SED. This has been recently demonstrated[?,?] for NGC 4151 and NGC 1068.

The idea behind this work[?,?] is the fact that different ions require different ionization energies and the observed spectrum is due to some weighted mixture of all those ions. The accurate knowledge of this mixture, based on the comparison of model calculations with observations, can be used to deduce the relative ionizing flux at each energy. This is illustrated in Fig. **??** that shows the ionization potential of several ions that are known to produce strong emission lines against the unobserved part of the SED. Obviously, there are other unknowns to do with the gas distribution, composition and amount of dust. However, the superb two dimensional spectroscopy provided by HST, combined with accurate IR line measurements, produces such a large number of observed emission lines, that the results are quite secured.

An interesting result of the work of Alexander and collaborators[?,?] is that, in the two cases studied, there is clear indication of an absorption feature in the SED, just above the Lyman limit. Such an absorption can be caused, for example, by a large covering fraction of optically thin gas that is situated either in the BLR or just outside it. This absorbing gas may be related to optically thin BLR gas, or the X-ray and UV absorption systems discussed in the following section. It gives another indication that the earlier picture of two isolated regions in AGN, the BLR and the NLR, is just a very poor approximation of a very complex emission region. Real AGN seem to be full of clouds and filaments, close to the center and very far from it, that sometimes obscure the ionizing radiation affecting the conditions in some other clouds. A proper name is the *messy emission line region.*

5 The Highly Ionized Gas

The final example that is treated here in detail is that of a high ionization gas in the BLR and/or the NLR. We do not specify the gas density (mostly because it is unknown) but consider the general case where it is some two or three orders of magnitude smaller than the density of the material in that region. In the BLR, this would mean $N_{\rm H} \sim 10^{7-8}$ cm^{-3} and in the NLR $N_{\rm H} \sim 10^{1-3}$ cm^{-3}. We also assume a column density which does not exceed the column density of the already discussed components. The resulting ionization parameter is two-to-three orders of magnitude larger than the corresponding BLR or NLR ionization parameter. The gas is exposed to the AGN radiation field and we expect strong absorption and emission features in the soft X-ray part of the spectrum. The relevant ionization parameter to use in this case is U(oxygen) and the component is named the *highly ionized gas* (HIG).

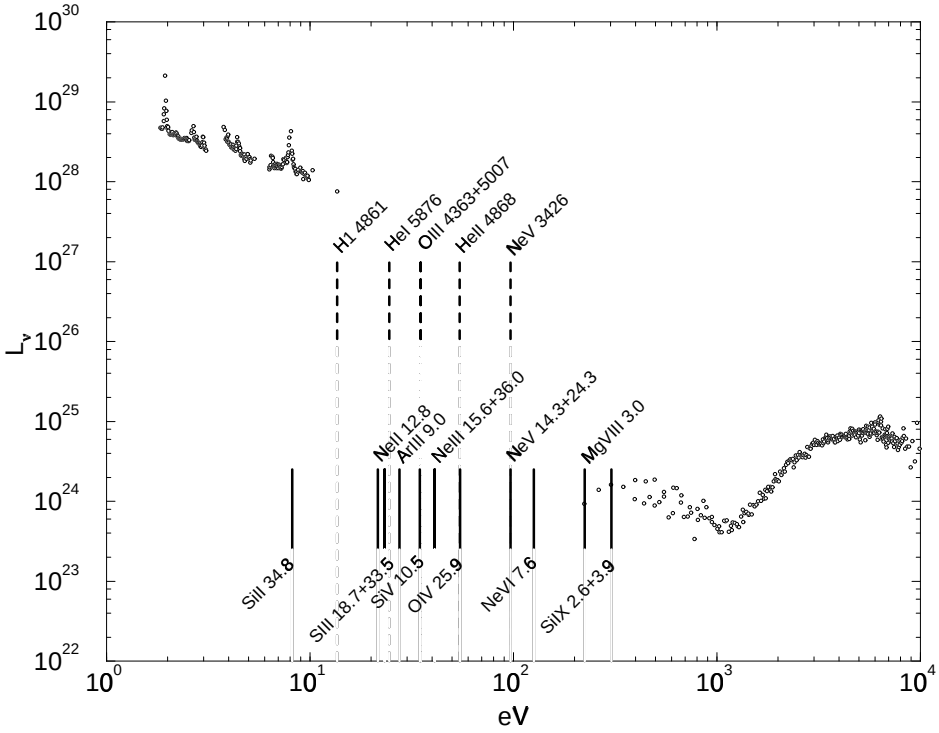

Figure 11. The unobserved part of the SED in AGN can be recovered by noting that various observed narrow lines are due to ions that require different ionization energies. The diagram shows some of the observed line ionization energies superimposed on the NGC 4151 continuum. From Alexander et al.[?] ©1999 AAS.

5.1 The Spectrum of the HIG

X-ray observations since the early 1990s show that many type-I AGN contain significant amounts of circumnuclear material which re-processes and modifies the intrinsic X-ray radiation. Partially-ionized X-ray absorbers were first suggested to exist in AGN in sources such as MR 2251-178 [?,?] and NGC 4151 [?,?]. Supporting evidence for such HIG (also referred to as "warm absorber") was also provided by *Ginga*, *ROSAT* and *BBXRT*. Study of the HIG spectrum has improved by the launch of *ASCA* that confirmed the already observed deficit

of photons close to ∼0.8 keV, soon to be interpreted as due to bound-free absorption by O VII and O VIII. Extensive studies of the feature, including its time-dependent behavior, can be found in several papers[?,?,?,?]. Such systems are very common in low luminosity AGN but seem to be less common in higher luminosity sources (a result that needs confirmation since observations of high luminosity sources are severely limited by the poor signal-to-noise ratio of the *ASCA* observations).

The X-ray spectrum of type-II AGN is completely different[?,?,?]. *ASCA* observations clearly show large EW lines (few × 100 eV) of H-like and He-like ions of neon, magnesium, silicon and sulfur, and weak X-ray continuum. The observed 0.5–10 keV luminosity is consistent with the standard model that involves obscuration by the central torus. The amount of obscuration can be directly measured in several type-II sources since the line-of-sight column is such that it is opaque to the very soft (∼ 1 keV) continuum yet transparent to the medium X-ray (∼ 5 keV) radiation. The material producing the large EW X-ray lines is not obscured, hence the large line-to-continuum intensity ratio. The HIG in type-II AGN is likely to have large dimensions and low density. It is not yet clear whether it is the same component observed in type-I AGN.

There are interesting suggestions about HIG which is far enough from the center to allow some dust particles to co-exist with the hot gas[?]. So far, there are only poor resolution *ASCA* data to support this idea while high resolution spectra, at around 0.5 keV (to detect the signature of neutral oxygen, the most abundant ion in the hypothetical dust) are required.

The study of HIG in active galaxies is being revolutionized by the new, high resolution spectra of the *Chandra* and *XMM* grating instruments. The handful of spectra already published shows rich emission and absorption features that confirm, in some cases, the earlier findings, but contradict others. An example is shown in Fig. **??** where the spectrum of NGC 3783, a type-I AGN with strong absorption features, is shown. The spectrum is clearly under-exposed but is good enough to illustrate the complexity of the features. Better spectra are expected soon.

Equally interesting are new *Chandra* observations of type-II sources[?,?] (see Fig **??**) that enables the very first measurement of the HIG extent. In those two sources (Mkn 3 and the Circinus galaxy) the HIG extends over tens to hundreds of parsecs.

X-ray emission and absorption lines are relatively easy to interpret. In general, we expect three generic type spectra:

Absorption dominated spectra are seen when the absorbing material is covering the entire source but the emission features are very weak since

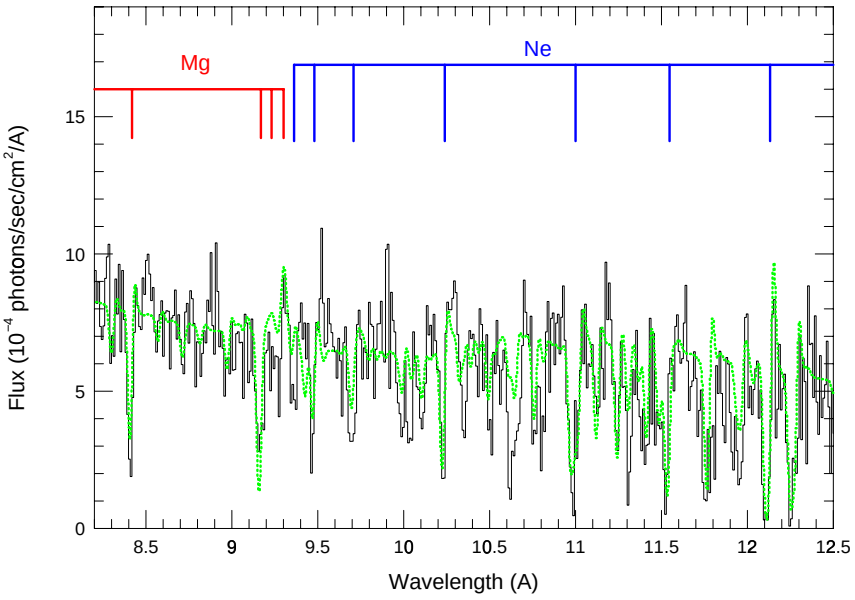

Figure 12. The spectrum of NGC 3783 as observed by *Chandra* (dark line) and a photoionization model fit to the data (light dotted line). All the absorption lines that are not marked are iron L-shell lines. Note the P-Cygni profiles of some lines. From Kaspi et al.[7]

there is little or no material on other sides (i.e. $C_f \ll 1$). An example is shown in Fig. **??**.

Emission dominated spectra are observed when the emitting gas is directly observed but the ionizing continuum is obscured. The spectrum is composed of X-ray lines and reflected (or scattered) X-ray continuum. As explained, the lines are mostly due to recombination in photoionized gas and due to collisional excitation in thermal plasma. The line EWs are normally very large because of the weak scattered continuum. An example is shown in Fig. **??**.

Emission and absorption spectra are seen in those cases where there is

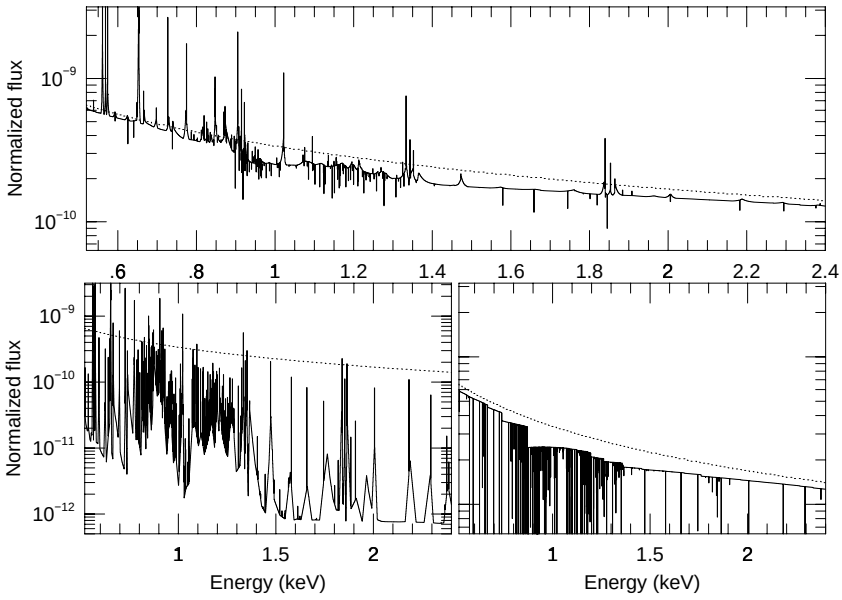

Figure 13. Pure absorption (bottom right), emission and reflection (bottom left) and combined (top) theoretical X-ray spectra of type-I AGN. The HIG is characterized by U(oxygen) = 0.03 and hydrogen column density of 10^{22} cm^{-2}. The dashed line is the incident continuum. Note the different energy scale on top and the different flux scale on the bottom left.

a direct view of the continuum, large covering fraction, large column-density HIG, and some gas on the line of sight to the center. The spectral appearance depends on various parameters. The ratio of the line-of-sight and total covering fractions determines the relative strength of the emission and absorption features. Relative motion, such as expansion, can result in P-Cygni type profiles and any azimuthal dependence in the gas properties can result in very different emission and absorption line intensities. Fig. **??** shows a combination of the absorption and emission spectra in a simple case where the HIG properties are the same on all sides of the source.

5.2 Where is the HIG?

The HIG is very different in its properties from the NLR and BLR gas. Its level of ionization is much higher and so is its covering fraction. It is therefore reasonable to assume that it occupies a much larger volume of space and the picture of small isolated clouds may not be valid in this case. In particular, the mass of this component may exceed, by much, the BLR and the NLR mass.

Unfortunately, so far there is no direct measurement of the HIG location and we can only parameterize its density mass and location by using the known U(oxygen) (~ 0.02) and column density. Scaling the HIG to the known BLR density, location and ionization parameter, and using the observed HIG column density, suggests that the HIG density is

$$N_{\rm HIG} \simeq 6 \times 10^6 \, L_{44}({\rm oxygen}) R_{\rm pc}^{-2} \ \ {\rm cm}^{-3}, \tag{24}$$

the physical thickness of a typical HIG cloud is

$$\Delta R_{\rm HIG} \simeq 5 \times 10^{-3} \, L_{44}^{-1}({\rm oxygen}) N_{22} R_{\rm pc}^{2} \ \ {\rm pc} \ , \tag{25}$$

and the mass of such clouds is

$$M_{\rm HIG} \simeq 10^3 \, N_{22} C_f R_{\rm pc}^{2} \ \ M_\odot \, , \tag{26}$$

where N_{22} is the hydrogen column density (assuming solar composition) in units of 10^{22} cm^{-2} and L_{44}(oxygen) the 0.54–10 X-ray luminosity in units of 10^{44} erg s^{-1} (for low luminosity AGN, like NGC 5548 and NGC 3783, $L_{44}({\rm oxygen}) \simeq 0.05$ and for the high luminosity quasars $L_{44}({\rm oxygen}) \simeq 1$). Given these properties, there are several likely locations for the HIG:

1. Just outside the central source, perhaps due to material blown away from the central accretion disk. In this case, the HIG density must be large, 10^{11} cm^{-3} or even larger.

2. Just outside the BLR, due to gas evaporation off condensations in the BLR. The condensations may be the high density cores of BLR clouds or bloated stars in the central star cluster. The blown-away gas, or wind, becomes transparent to the X-ray radiation and is pushed outwards by radiation pressure. Close to the outer BLR boundary, the density is about 10^8 cm^{-3}.

3. Well outside the BLR, occupying the same volume as the NLR. The density of this gas is very low and its mass extremely large (Eqs. **??** and **??**). Its origin is not clear, but so is the origin of the NLR gas. Such gas can directly be observed by *Chandra* (as shown, already, in two cases).

Obviously, there is nothing to against the possibility of more than one origin or location.

Regarding the largest region, it has been suggested[?] that the HIG is, in fact, the coronal line region gas. The few available calculations suggest that the level of ionization is similar (yet not identical) and the IR and X-ray observations may represent the same phenomenon. This interesting suggestion is currently under investigation.

5.3 The Motion of the HIG

The high level of ionization makes the HIG subject to strong radiation pressure force. In this respect, there is a major distinction between this component and the colder BLR and NLR gas. We therefore expect the HIG to flow out of the system with velocities that depend on the "launching" location of the flowing gas (the attained velocity is typically of the same order of magnitude as the escape velocity at the base of the flow), the run of external pressure as a function of radius, and the micro-physics of the gas. The micro-physics determines the value of the force multiplier (see Sec. 2.9) and the local acceleration. Additional factors are the ionization level, the metal abundance and the internal motion (microturbulence) that controls the contribution of bound-bound transitions to $M(r)$. Recent calculations indicate that $M(r) \sim 10$ if the internal motion is of the order of the sound speed in the gas. This means that sources with $L/L_{Eddington} > 0.1$ can efficiently accelerate HIG clouds.

It is not yet clear whether the term "cloud" used for the colder components (and required to explain the optical-UV observations) can be applied to the HIG. While high ionization clouds can form in a medium controlled by external magnetic pressure, or pressure due to very high temperature material, they may not survive long enough to show the observed spectral features. The existence of such clouds is still an open question that may be resolved by new X-ray observations. Alternatively, the HIG may be an outflowing wind that requires no confinement. This would fill large volumes of space and is less likely to produce multi-component absorption systems. Fig. **??** shows new calculations[?] for the velocity of HIG clouds under various conditions. So far, there is no detailed study of the complementary case of a wind-type HIG.

5.4 Associated UV absorbers

UV spectroscopy of type-I AGN clearly shows narrow absorption lines that are usually blueshifted with respect to the BLR velocity. These are most

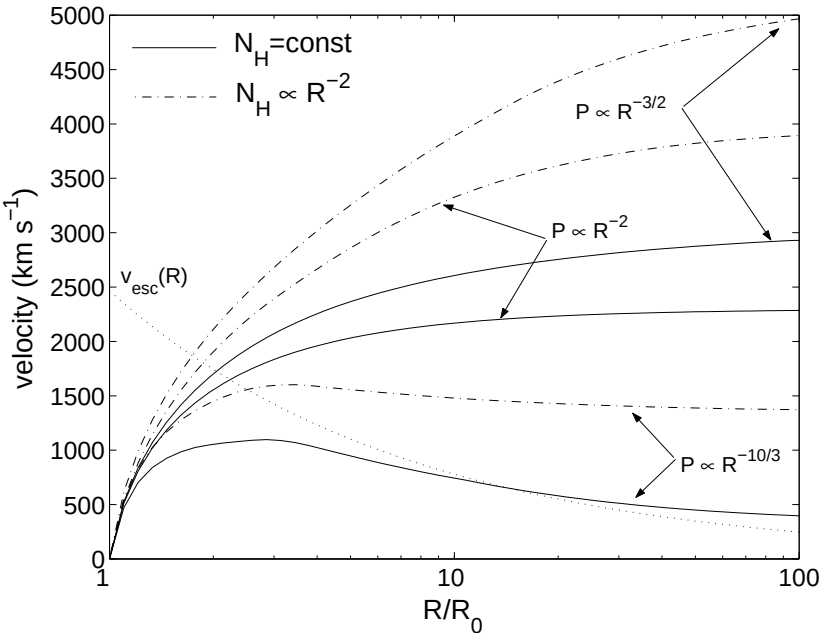

Figure 14. Calculated velocities of HIG clouds under various conditions of external pressure, P, as marked. The dotted line gives the escape velocity at the various locations. From Chelouche & Netzer[?] ©2001 Blackwell Sci.

probably caused by intrinsic outflowing gas. Another well known example is the broad absorption lines (BALs) that will not be discussed here.

Narrow intrinsic AGN absorption lines span a wide range of ionizations, from O VI and Ne VIII to C II, Mg II and Si II. Intrinsic QSO absorbers are not very common. They can have single or multiple line components, velocity shifts from near 0 km s^{-1} to many thousands km s^{-1}, and velocity widths from near the thermal Doppler speed to at least[?] several hundred km s^{-1}. Intrinsic absorption lines appear in a large fraction (∼50%) of type-I AGN. The lines are typically highly variable, a few hundred km s^{-1} wide, and blueshifted by about 500–1500 km s^{-1} from the emission redshift[?,?].

Recent studies of type-I AGN led to the suggestion that the presence of UV line and X-ray continuum absorptions are correlated[?,?]. The extreme view of this model is the speculation that the two absorption phenomena occur in the same gas. Photoionization calculations have shown that, in some cases,

the column densities measured from the UV and X-ray features are consistent with a one-component absorber[?,?,?,?]. In these models, the ions producing the low- to moderate-ionization UV lines, such as C IV λ1549 and N V λ1240, are just trace constituents in a gas dominated by O VII, O VIII, Ne IX and Ne X. Other cases, showing incompatible conditions[?] are known too and it is quite likely that, in many sources, both originate in very different clouds.

While it is not yet clear whether the HIG gas is related, in any way, to the coronal line region, or the gas producing the intrinsic UV absorption lines, its observation re-enforces the view presented earlier that the picture of distinct isolated regions is not valid any more. Instead, we should adopt the more realistic view of a "messy AGN" in which clouds of different types exist in many different locations. Some are of high enough density to produce a typical $T_e \sim 10^4$ K photoionized gas spectrum while others are of lower density, higher temperature and higher level of ionization. It is not yet clear what dominates the motion of the BLR and NLR gas but it is clear that the lower density HIG is moving out of the system, being pushed, most likely, by radiation pressure force.

5.5 Time Dependent HIG?

The HIG in AGN is subjected to a highly variable continuum source. Depending on the gas density and temperature, the emergent spectrum will be time dependent. We can estimate the location of the HIG where such short-time effects will become noticeable. For example, in type-I AGN, the ionization parameter is well constrained and the location and density of the gas are simply related (Eq. **??**). A recombination-time vs. distance relation can be established. For example, the typical few hours time variability of many type-I AGN will result in variable X-ray lines if the HIG distance is 0.1 pc or less.

The investigation of time dependent photoionization of the HIG gas is just starting[?,?]. The observational work is also in a preliminary stage. *Chandra* and *XMM* are definitely capable of determining the HIG location using reverberation studies of X-ray emission lines, similar to the reverberation mapping of the BLR, and measuring variable absorption lines. The next couple of years is likely to see the answer to this question.

Even if the HIG is further out, and the density is smaller, much longer time scale variations (years!) are known to occur in AGN and the presently observed X-ray spectrum may reflect past very bright or very faint phases of the source. HIG models must take this into account.

Table 2. AGN components: locations and densities

Component	*location*	*density*
Accretion disk	10^{-3} pc	$\sim 10^{15}$ cm^{-3}
BLR	0.01-0.1 pc	$\sim 10^{10}$ cm^{-3}
Torus	1–10 pc	10^{3-6} cm^{-3}
Warm absorber	?	10^{2-10} cm^{-3}
NLR	100–1000 pc	10^{3-5} cm^{-3}
Starburst	$\sim$ 1000 pc	10^{0-4} cm^{-3}

5.6 Other X-ray Bright Components

The X-ray bright components in AGN are those clouds, or condensations, that are exposed to the direct radiation field of the central continuum source and where U(oxygen) is large enough for the H-like and He-like ions of most metals to be the most abundant ions. Since the location and the density of most components, except the HIG, are roughly known, we can check each of those, in turn, to see whether it can contribute to the observed X-ray spectrum. Using the previously defined L_{44}(oxygen) and assuming a typical $\gamma_{\rm X} = 1$, we estimate

$$U(\text{oxygen}) \simeq 0.2 L_{44}(\text{oxygen}) R_{\rm pc}^{-2} N_5^{-1} \ , \qquad (27)$$

where $N_5 = N_{\rm H}/10^5\,{\rm cm}^{-3}$. A list of components is given in Table **??**. As evident from the combination of Eq. **??** and Table **??**, the central molecular torus, if it exists with dimensions and density as assumed in standard AGN models[7], is a likely strong X-ray source. The level of ionization of the inner torus walls can be high enough to produce X-ray lines, and the column density large enough to reflect a large fraction of the incident continuum. The expected covering fraction of the inner torus walls exceeds 50% (see Goodrich in these proceedings) so the reflected continuum can contribute significantly to the observed X-ray flux.

The uncertainty in the inner torus density is large enough to prevent us from making detailed predictions. At the high density range, most of the gas is almost neutral and X-ray reflection is inefficient. The resulting reflected X-ray continuum is very hard and the iron Kα line is dominated by low ionization iron. The central energy of this feature is around 6.4 keV and we expect a low-contrast Compton scattering shoulder that extends the line profile to lower energies. At the low density limit, the gas is more ionized and the emission line spectrum dominated by H-like and He-like species. Obviously, the above description is highly simplified since the X-ray flux itself can affect

the inner-wall density by producing winds and by causing low density material to evaporate off the inner surface.

6 The AGN-starburst Connection

6.1 Star-Forming Regions in AGN

Several type-II AGN show nuclear star-forming rings or bright nuclear HII regions. The X-ray band is probably most suitable to investigate and identify this activity, because of the large expected X-ray luminosity, as a result of fast stellar winds and supernovae explosions. Extended soft X-ray emission, which is most probably due to starburst activity, has already been observed in the inner $\sim$1 kpc region of many such sources (e.g.[?] NGC 1068). The phenomenon is very common – indeed there are only a few sources where this is *not* observed.

The difference between "pure" starburst activity and the one observed in active galaxies is the presence of the central, powerful X-ray source. Keeping in mind the definition of U(oxygen), we can assess the influence of this source using the known location and the expected density of the star-forming regions. This is given in Table **??** and Eq. **??**. Evidently, under reasonable assumptions, the central X-ray source must influence and modify the physical properties of the starburst produced gas.

Finally, the suggestion that high accretion rates in luminous AGN may be related to high column of nitrogen enriched material, whose origin is nuclear starburst[?,?] may or may not be related to this question.

6.2 The X-ray Spectrum of Star-Forming Regions

"Pure" starburst galaxies (e.g. NGC 253) show the typical X-ray signature of supernova explosions and fast stellar winds, and the high velocity flows and dusty condensation observed in star forming regions. The X-ray signature is of a hot ($kT \sim 0.3 - 2$ keV) plasma, with its typical free–free continuum and several large ($\geq$100 eV) equivalent width emission lines[?,?]. Extreme starburst activity is associated with so-called *superwinds*[?] that are observed at both optical and X-ray energies. The X-ray emitting regions of starburst regions are spatially resolved, showing typical dimensions of order one kpc. The pre-*Chandra* and *XMM* abundance determinations, using the X-ray lines, were problematic since they implied extremely low metallicities, in clear contrast to the theoretical expectations and the optical-IR-UV measurements. These may be traced to wrong identification of the low resolution instruments.

As noted in Sec. 2, the spectrum of low density, low opacity collisional plasma is determined by the gas temperature and composition. Accurate calculations of pure thermal gas are widely available and the only significant unknowns are certain atomic data (most notably, the collision strengths and dielectronic recombination rates of iron M-shell and L-shell lines). Since the level of ionization is uniquely defined by the gas temperature, the latter can be found by comparing the intensity of lines from different ions, for a given metal abundance. One can thus construct line ratio and diagnostic diagrams, similar to those shown in Fig. **??**, where the independent variable is the temperature, rather than the ionization parameter. An example is shown in Fig. **??**. Observing a number of X-ray lines of different species, and using such diagrams, allows to solve for both the gas temperature and composition. Obviously, this single temperature view of the starburst gas is over simplified and can only be used as a first approximation to the more complex real situation.

6.3 Starburst Galaxies and ULIRGs

The term *starburst galaxies* used here refers to one of two cases. The first is the "pure" starburst galaxy described in Sec. 6.2. Such object shows no clear central radiation source and the gas micro-physics is controlled by collisional processes. The second category includes the Ultra Luminous IR Galaxies (ULIRGs) that are characterized by very high IR luminosity ($> 10^{45}$ erg s^{-1}) and extreme extinction ($A_V \sim 50 - 100$ mag). The main power house of ULIRGs is completely obscured from view and the observed luminosity is due to thermal emission by the hot dust. Most ULIRGs show clear star forming activity but some also show signs of accretion onto a massive black hole. ULIRGs are thought to be the result of mergers[?], an idea that is clearly supported by recent HST near-IR imaging.

Galactic merger can lead to several different results. First, it can trigger violent star-forming activity including heating of the ISM to X-ray energies and large scale outflows with typical velocities[?] of ~ 1000 km s^{-1}. Second, it can result in the formation of giant black holes (or, alternatively, in fast growing of small existing black holes) during the merging event. This may eventually lead to the formation of high luminosity AGN. The two can proceed along different tracks but can also operate, side by side, in the very same merger.

The observational manifestation of a galactic merger is different for different cases and depends, also, on the stage of the merger. In particular, there is an interesting on-going debate about the main power source of several dozens of observed ULIRGs which can be either the violent star formation (producing

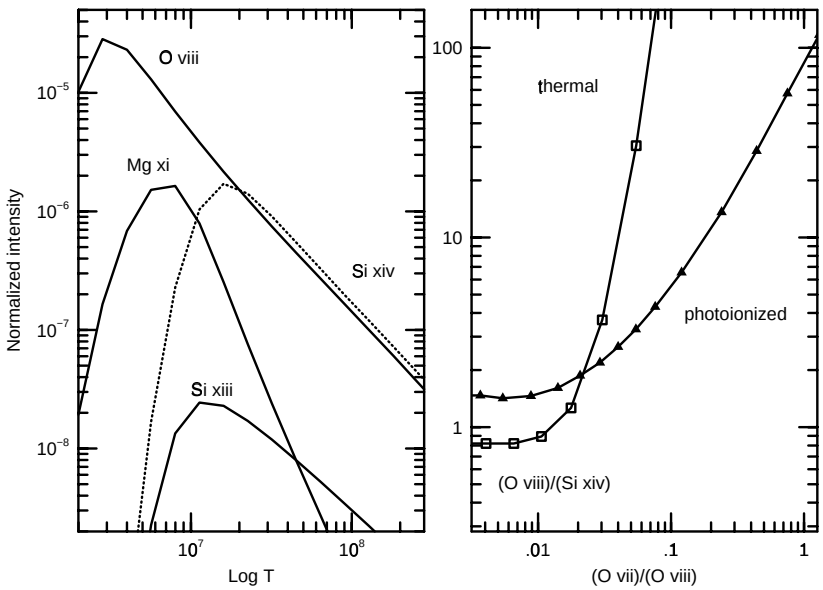

Figure 15. Left: line ratio diagram, for several intense X-ray lines, in a low density ($N_{\rm H} = 10^3$ cm^{-3}) solar metallicity, optically thin collisional plasma. Right: A diagnostic diagram showing, this time, the thermal gas line ratio (left curve with squares; the temperature is increasing from top to bottom) along side the photoionized gas curve (marked with triangles) from Fig. **??**

star clusters that are more luminous than many quasars!) or the newly formed central AGN. While the spectroscopic signatures of the two are predicted to be very different, the analysis is extremely complicated since the optical-UV part of the spectrum is completely obscured by dust, and the standard line emission diagnostics cannot be used. Only two spectral bands are available for a detailed study, the hard X-ray band and the mid-to-far IR band.

Genzel et al.[?] suggested several diagnostics to identify the main source of energy. They are based on the level of ionization of the IR lines and the intensity of the PAH features. For example, only AGN type continuum can

ionize oxygen beyond O^{+2} thus a strong O IV line is a clear AGN signature. As for the PAHs, such molecular features are easily destroyed by the intense, high energy radiation field of an AGN. Strong PAH is thus evidence for the absence of a powerful AGN.

There is a simple way to test for the existence of a central AGN in ULIRGs using hard X-ray observations. At this energy ($\sim 3-10$ keV), the large obscuring dusty material becomes transparent, in some sources, and the central source can be directly observed. Indeed, X-ray observations clearly show a powerful central AGN-type source in several ULIRGs, on top of soft (0.5-2 keV) nuclear sources that can be due to the starburst activity. In some cases, the power-law X-ray source is associated with IR lines from highly ionized gas. This gas (which is, in fact, the NLR) must be exposed to a strong central UV source in order to emit such lines. However, in several sources, like[?,?] NGC 6240, there is no indication of highly ionized species in the IR and the only AGN signature is in the X-ray band (in the case of NGC 6240, the X-ray source is obscured by a huge column of column of $\sim 10^{24}$ cm^{-2}). Such cases defy standard explanation. One possibility is that the obscuring material covers the entire source and there is no cone through which the NLR gas, if exists, can be ionized. The observed low excitation IR lines are emitted, in this case, by star-forming regions outside the central obscurer.

6.4 A Combined Model

The properties of the X-ray emitting gas in several ULIRGs must be governed by both large scale dynamical processes (mergers and star-forming activity), as well as by the strong radiation field of the central AGN. Modeling them as pure photoionized regions regions that are excited by a single central source, or as pure collisionally ionized plasma in extended star-forming regions, is clearly oversimplified. Understanding the sources, and the overall AGN-starburst relationship, requires more sophisticated models, combining thermal and photoionization excitations. This is true in particular in those ULIRGs where the central AGN is powerful enough and the star-forming regions are close enough to the nucleus. In such cases, collisional excitation together with photoionization is affecting the physical conditions in the observed X-ray gas. The analysis of such spectra requires new and advanced diagnostic tools.

Fig. **??** shows two spectra. One is a standard $T = 10^7$ K stationary collisional plasma and the other the spectrum of this gas when illuminated by a power-law X-ray continuum similar to the one expected from a central AGN, assuming $U(\text{oxygen}) = 0.2$. The spectral appearance of the two is

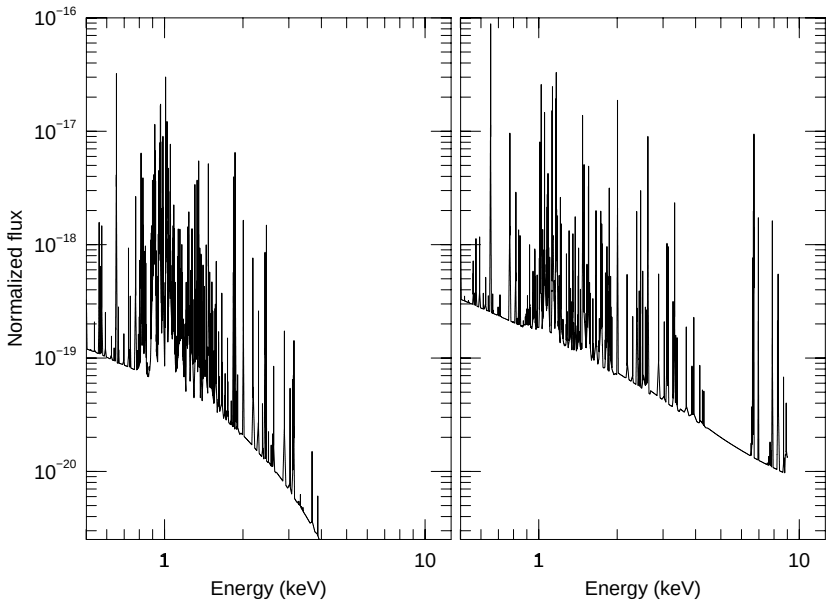

Figure 16. Left: The spectrum of a steady state $kT = 1$ keV collisional plasma. Right: The spectrum of the same $kT = 1$ keV plasma when illuminated by a central AGN source with U(oxygen)=0.2. Note the absence of strong iron lines in the pure collisional case.

very different. While the pure thermal plasma continuum is curved, and the high ionization lines of H-like and He-like iron, around 6.7-7 keV, are weak or absent, this is not the case when photoionization is taken into account. A clear signature of the photoionized gas is the flat continuum and the strong ionized iron lines. Present day X-ray spectroscopy can distinguish between the two possibilities provided adequate theoretical tools are available. The observations can supply the location of the line emitting gas, the luminosity and SED of the X-ray source and the high resolution spectra. New diagnostic diagrams, especially prepared for analyzing such cases, taking into account both excitation processes, must be developed. They will use the observed line ratios to deduce the value of U(oxygen), the gas temperature and composi-

tion, and the effect of stellar winds and central radiation pressure on the gas dynamics. X-ray observations and analysis provide a new way, perhaps the most efficient and meaningful one, to understand ULIRGs and the physics of star-forming regions near powerful, AGN-type sources.

Finally, it must be re-emphasized that the gas in starburst galaxies, in star-forming regions in AGN and in ULIRGs, may not be stationary or in steady state equilibrium. The single temperature stationary plasma models illustrated here, give only the zero order approximations for a more complex situation. New, time-dependent non-stationary models must clearly be developed to fully understand some of these objects.

7 Open questions

Throughout this review we have mentioned several outstanding questions regarding the standard AGN model, starburst galaxies and the AGN-starburst relationship. A list of this type is necessarily long and I will make no attempt to present a complete one. The following is a summary of some of the questions that were addressed here:

- What is the nature of AGN clouds? Are they bloated stars or smaller condensations confined by external pressure? What is the number of clouds and their radial distribution? What is the origin of the confining pressure?

- What is the mass budget of AGN? What is the ratio of the accreted mass to the outflowing mass?

- What is the resolution of the energy budget problem and what is the "real" SED?

- How realistic is the simple two-zone model of AGN low temperature gas (BLR and NLR)? Is there an *intermediate line region* and what is the reason for its low emissivity? What is the role of dust in all emission line regions?

- What is the global dynamics of the NLR gas? Is the outflowing model with central obscuration observed in NGC 4151 and NGC 1068, typical of other source?

- How common are central absorbers (i.e. the material between the center and the NLR)? What is their effect on the NLR spectrum?

- What is the location, the mass and the motion of the HIG in type-I AGN? Is it the same component producing the UV absorption lines and what is the relationship with the coronal line region?
- What are the properties of the HIG in type-II AGN? Is it the same component producing the $\sim$1 keV absorption in type-I AGN? Can the apparent differences between type-I and type-II objects be fit into a single unified scheme?
- What are the physical properties of the X-ray emitting gas in starburst galaxies not hosting luminous AGN? What is the composition of this gas?
- What is the dominant excitation mechanism of the HIG in ULIRGs and starburst galaxies hosting luminous AGN: mechanical heating, photoionization by the central radiation, or both?
- Is the X-ray emitting gas in nuclear starburst region showing type-II AGN influenced mainly by the starburst activity or the central radiation field? Is the spectrum time dependent and on what time scale? Is the motion of this gas influenced by the central radiation field?

Acknowledgments

This work is supported by the Israel Science Foundation and by the Jack Adler Chair of Extragalactic astronomy.

References

1. Alexander, T., MNRAS, 285, 891, 1997.
2. Alexander, T., & Netzer, H., MNRAS, 270, 781, 1994.
3. Alexander, T., & Netzer, H., MNRAS, 284, 967, 1997.
4. Alexander, T., Strum., E., Lutz, D., Sternberg, A. Netzer, H., & Genzel, R, ApJ, 512, 204, 1999.
5. Alexander, T., Lutz, D., Strum., E., Genzel, R., Sternberg, A. & Netzer, H., ApJ, 536, 710, 2000.
6. Antonucci, R., ARAA, 31, 473, 1993.
7. Arav, N., Barlow, T., Laor, A., Sargent, W.L.W., & Blandford, R.D., 297, 990, MNRAS, 1998.
8. Baldwin, J.A., ApJ, 214, 679, 1977.
9. Baldwin,J.A., Ferland, G.J., Korista, K. & Verner, D., ApJL, 445, L119, 1995.

10. Bicknell, G.V., Dopita, M.A., Tsvetanov, Z.I., & Sutherland, R.S., ApJ, 495, 680, 1998.
11. Binette, L. & Robinson, A., A&A, 177, 11, 1987.
12. Bottorff, M. C., & Ferland, G.J, ApJ, in press.
13. Chelouche, D., & Netzer, H., MNRAS, in press.
14. Clavel, J. et al., A&A 357, 839, 2000.
15. Crenshaw, D.M., Kraemer, S.B., Bogess, A., Maran, S. P., Mushotzky, R.F., & Wu, C., ApJ 516, 750, 1999.
16. Dopita M. & Sutherland, R.S., ApJ, 455, 468, 1995.
17. Edwards, A. C. , MNRAS, 190, 757, 1980.
18. Emerson D. in "Interpreting Astronomical Spectra", John Wiley and Sons, 1997.
19. Emmering, R.T., Blandford, R.D., & Shlosman, I., ApJ, 385, 460, 1992.
20. Eracleous, M., Livio, M., & Binette, L., ApJL 445, L1, 1995.
21. Fabian, A., Kunieda, H. Inoue, S. Matsuoka, M. Mihara, T. Miyamoto, S., Otani, C. Ricker, G., Tanaka, Y., Yamauchi, M., & Yaqoob, T., PASJ, 46L, 59F, 1994.
22. Ferguson, J.W., Korista, K.T., & Ferland G.J., ApJS, 110, 287, 1997.
23. Fiore, F., Perola, G. C., & Romano, M., MNRAS 243, 522, 1990.
24. Genzel, R., et al., ApJ 498, 579, 1998.
25. George, I.M., et al., ApJS 114, 73, 1998.
26. Guanazzi M. et al., MNRAS, 310, 10, 1999.
27. Halpern, J.P., ApJ, 281, 90, 1984.
28. Hamann, F., & Ferland, G.J., ApJ, 418, 11, 1993.
29. Hamann, F., & Ferland, G.J., ARAA, 37, 487, 1999.
30. Hamann, F.W., Netzer, H., & Shields, J.C., ApJ 536, 101, 2000.
31. Heckman, T., et al., ApJ 457, 616, 1996.
32. Iwasawa, K., MNRAS 302, 961, 1999.
33. Kaspi S. & Netzer, H. ApJ, 524, 71, 1999.
34. Kaspi, S., Smith, P.S., Netzer, H., Maoz, D., Jannuzi, B.T., & Giveon, U., 1999, ApJ, 533, 631, 2000.
35. Kaspi, S., Brandt, W.N., Netzer, H., George, I.M., Chartas, G., Behar, E., Sambruna, R.M., Garmire, G., & Nousek, J.A., ApJ, submitted.
36. Kazanas, D., ApJ, 347, 74, 1989.
37. Komossa, S., & Breitschwerdt, ApJS, 272, 299, 2000.
38. Korista, K. T., Ferland, G.J., & Baldwin, J., ApJ 487, 555, 1997.
39. Korista, K. T. & Goad, M. R., ApJ, 536, 284, 2000.
40. Kraemer, S,B. & Crenshaw, D.M., ApJ, 532, 256, 2000.
41. Krolik J. "AGN" , Princeton Series in Astrophysics, 1999.
42. Krolik, J.H., McKee, C.F., & Tarter, C.B., ApJ, 249, 422, 1981.

43. Krolik J. & G. Kriss, ApJ, 447, 512, 1995.
44. Laor A., ApJL, 496, L71, 1998.
45. Maran, P.S., Crenshaw, D.M., & Mushotzky, R.F., ApJ, 465, 733, 1996.
46. Mathews, W.G., & Ferland, G., J., ApJ, 323, 456, 1987.
47. Mathur, S., ApJ, 431, L75, 1994.
48. Mathur, S., Wilkes, B., Elvis, M., Fiore, F., ApJ, 434, 493, 1994.
49. Matt, G., Brandt, W. N., & Fabian, A.C., MNRAS, 280, 823, 1996.
50. Mihalas, D., "Stellar Atmospheres" , W.H. Freemen and Company, 1978.
51. Nandra, K., Pounds, K., Nat, 359, 215, 1992.
52. Netzer, H., ApJ, 289, 451, 1985.
53. Netzer, H., in Active Galactic Nuclei, Courvoisier & Mayor eds., Berlin:Springer, p57, 1990.
54. Netzer, H. , ApJ, 473, 781, 1996.
55. Netzer, H., & Laor, A., ApJ, 404, L51, 1993.
56. Netzer, H., Turner,T.J., George,I.M., ApJ, 504, 680, 1998.
57. Nicastro, F., Fabrizio, F., Perola, G.C., & Elvis, M., ApJ, 512, 184, 1999.
58. Osterbrock D.E. "Astrophysics of Gaseous Nebulae and Active Galactic Nuclei", University Science Books, 1989.
59. Pan, H., Stewart, G.C., Pounds, K.A., MNRAS, 242, 177, 1990.
60. Penston, M.V., MNRAS, 233, 601, 1988.
61. Peterson, B.M. "An Introduction to Active Galactic Nuclei", Cambridge University Press, 1997.
62. Porquet, D, Dumont, A.M., Collin, S, & Mouchet, M., A&A 341, 59, 1999.
63. Ptak, A., Serlemitsos, P., Yaqoob, T., Mushotzky, R.., ApJS, 120, 179, 1998.
64. Rees, M.J., MNRAS, 228, 47p, 1987.
65. Reynolds, C., MNRAS 286, 513, 1997.
66. Reynolds, C.S., Fabian, A.C., Nandra, K., Inoue, H., Kunieda, H., & Iwasawa, K., MNRAS, 277, 901, 1995.
67. Robson I., "Active Galactic Nuclei", John Wiley & Sons, 1996.
68. Sako, M., Kahn, S.M., Pharels, F, & Liedahl, D.A., ApJL, 543, L115, 2000.
69. Sambruna, R. M., Netzer, H., Kaspi, S., Brandt, W. N., Chartas, G., Garmire, G. P., Nousek, G. A., Weaver, K. A., ApJL, in press.
70. Sanders, D., Mirabel, F., ARAA, 34, 749, 1997.
71. Scoville, N., & Norman, C. , ApJ, 332, 163, 1988.
72. Shields, J., & Hamann, F., ApJ 481, 752, 1997.
73. Strum, E., Alexander, T., Lutz, D., Sternberg, A. Netzer, H. & Genzel, R, ApJ 512, 197, 1999.

74. Turner, T.J., et al., ApJ, 488, 164, 1997.
75. Veilleux, S., ApJS, 75, 357, 1991.
76. Vignati, P., et al. A&A 349, l57, 1999.
77. Wills, B.J., Laor, A., Brotherton, M.S., Wills, D., Wilks, B.J., Ferland, G.J., & Shang, Z., ApJL 515, L53, 1999.
78. Wilson, A., & Elvis, M., Ap. Sp. Sci., 248, 14, 1997.
79. Wilson, A.S. & Raymond, J.C., ApJL, 513, L115, 1999.
80. Yaqoob, T., & Warwick, R. S., MNRAS, 248, 773, 1991.
81. Zheng, W., Kriss, G.A., Telfer, R.C., Grimes, G.P., & Davidsen, A.F., ApJ 475, 469, 1997.